Vibration Interferences in the Limited Orbital Field of Sea Waves in Theory and Physical Model

Elliptic wave theory

The influence of the phase difference Δφ between incident and reflected linear waves on the transformation of partially standing waves, in the area of changing inclination of the sea ground.

By FRITZ BÜSCHING
(http://orcid.org/0000-0002-6673-8273)

Summary

The movements in the orbital field of water waves of unlimited and limited water depth are attributed to the interaction of their transverse and longitudinal vibration components. In contrast to the linear wave theory and to higher order theories too, in which the continuity condition is also not fulfilled, a reflection process is assumed concerning the description of the wave transformation due to decreasing water depth.
On the one hand, reference is made to the definition of the complex reflection coefficient $\Gamma = C_r e^{i\Delta\varphi}$ (CRC), according to Büsching (2012) [1], whose characteristics represent the consideration of the phase difference Δφ between the incident and the reflected wave. On the other hand, the method of "exponentially reduced reflection" that Schulejkin (1956) [2] used regarding the horizontal floor, which fulfills the condition of continuity, is extended to the range of floor slopes $0^o \leq \alpha \leq 90^o$.
Accordingly, two theoretical boundary conditions are assumed: On the one hand, the positive Clapotis, the characteristic of which is a linearly polarized vertical transverse oscillating movement in the antinode (or on a vertical wall of slope inclination $\alpha = 90^o$), and on the other hand the negative Clapotis, which is characterized by a linear polarized horizontal rocking motion on the bottom ($\alpha = 0^o$) of a shallow sea.
The observable forms of formation of partially standing waves (interference phenomena) are attributed *a priori* to the phase differences mentioned (phase jumps Δφ). The latter in turn depend on the inclination of the seabed near the coast. The phase shift Δφ given by the slope inclination α determines the positioning of the *rotated elliptical orbital paths* on inclined slopes in the surf zone. Apart from superimposed drift flow and non-linear compression effects in nature, the shape and inclination of such predictable orbital paths should be decisive for the formation of the different forms of breaking waves. The washing movement that occurs after wave breaking (wave run-up and run-down) corresponds approximately to the linearly polarized swinging movement of the negative Clapotis.
In addition to the continuity condition that has now been fulfilled, the consideration of the phase shift Δφ probably means, that a further link that was previously missing to describe the wave transformation due to decreasing water depth has been found. If necessary, a future consideration of the phase shift Δφ could also mean a paradigm shift in surf research including the tsunami problem, even with non-linear theories.

Keywords

Phase Jump, complex reflection coefficient (CRC), partial Clapotis, orbital velocity of water waves, exponentially reduced reflection (ERR).

Preface

This version of this article was intended for the student readers of my "Coastal Engineering Repetitorium" (http://hydromech.de). For these, the multiple explanations of similar contexts still contained are likely to be more helpful than superfluous. An appropriately shortened text, also intended for publication, is in preparation. It is recommended that you read Chapters 1 and 14 first. Due to incorrect translation from German, at some positions the comma is used instead of the dot in mathematical expressions.

https://doi.org/10.24355/dbbs.084-202002031131-0

Contents

1. Detailed summary

Caused by *wave resonances* observed in nature and model on *steep shore formations* on the one hand and by phase jumps on moderate to *flat-inclined embankments* on the other hand, the author had defined the reflection coefficient as a complex quantity [1], [3]

The objectives of this article are:

- Securing the theoretical and practical findings regarding the complex reflection coefficient (CRC) using the example of model studies carried out in the wave channel.
- The explanation of the wave transformation in the delimited coastal orbital field a *priori* as an interference phenomenon, caused by slope-dependent phase jumps.
- To contribute to the awareness of the spectral analysis methods used by the author, and to present their advantages in terms of the description of the near-surface deformation processes of the waves.

https://doi.org/10.24355/dbbs.084-202002031131-0

Oriented on the linear wave theory (Airy-Laplace), the author assumes the verified decrease in the orbital circle diameter with the water depth according to the known exponential law but uses only the basic trigonometric functions in linear vibration theory.

The orbital field considered comprises on the one hand the wave movements generated at the interface water-air (water level deflections (WLD) and on the other hand fixed boundaries with different inclinations. The transformation of the waves in the range of decreasing water depth is treated a priori as a reflection problem, whereby the place of reflection depends on the inclination of the fixed boundary.

As an incident wave of height $H_i = 1$, the kinematics of the deep-water wave is used as a cosine wave.

The author puts the orbital velocities in the foreground of his investigations and includes phase shifts $0^o \leq \Delta\varphi \leq 180^o$ and slope inclinations $0^o \leq \alpha \leq 90^o$ in the view, referring to the definition of the complex reflection coefficient CRC. In addition, the mirroring method used by (Schulejkin, 1960 [2]) with regard to the kinematics of a shallow sea with a horizontal seabed is taken into account. This is extended by the author to inclinations $0^o \leq \alpha \leq 90^o$ and is referred to by the term "exponentially reduced reflection (mirroring)" (ERR).

Chapter 5: In the most well-known example of the total reflection of water waves on an ideally smooth vertical wall, in which there is no phase difference between incoming and reflected waves ($\Delta\varphi = 0^o$) particularly the linearly vertically polarized particle vibration in the edge streamline is taken into view. In the case of unlimited water depth at the wall, the term "positive (deep water) Clapotis" is used in a more precise way. On the other hand, in a shallow sea in the (flat inclined) edge streamline (on the ground), a linearly polarized particle oscillation arises, which is here referred to as the appearance of the "negative (flat water) Clapotis". The latter is created analogously to the positive Clapotis by a horizontal mirroring, but with a phase jump of $\Delta\varphi = 180^o$. Both Clapotis types are considered as theoretical boundary structures, the former appearing as a transversal oscillation with double maximum amplitude and the second as longitudinal oscillation with double maximum elongations.

Chapter 7: For the general case of reflection on inclined flat surfaces the relationship between horizontal phase displacement $\Delta\varphi$ and slope inclination α

$$\Delta\varphi = 180° - 2\alpha$$

has been found by the author.

The applicability of the above equation is impressively demonstrated by the degree of consistency with the results of the relevant model studies, which the author had already reported on in 2013 as part of the definition of the CRC:

For the slope of inclination studied in the hydraulic model 1:n = 1:2 (corresponding to $\alpha = 26{,}57^o$ or $\Delta\varphi = 126{,}86^o$) the phase shift between the incident and the reflected wave was calculated there, with respect to a partially standing “Partial wave” of an energy spectrum, as an arithmetic mean:

$$\Delta\varphi = \frac{132.6°+123.2°}{2} = 127.9° \approx 126.86^0.$$

The comparable values to be averaged for the $\Delta\varphi$ were taken into account, considering the different distances of the (imperfect) antinodes η_{max} or nodes η_{min} distant from the intersection (IP) of the slope with the still water level.

https://doi.org/10.24355/dbbs.084-202002031131-0

Chapter 8: According to the application of the ERR, the waves coming in from the deep water at circular orbital velocities are superimposed on the exponentially reduced mirrored circular orbital velocities of the reflected waves with opposite rotational sense.

This is realized here by the fact that 8 (or 16 respectively) orbital circle vectors regularly distributed on the circumference of the orbital circle of the incident waves are superimposed with the respective exponentially reduced mirrored ones. Analogous to the superimposition of potential currents, the tangents of the resulting orbital orbits are obtained as a result on the one hand and the corresponding orbital velocity magnitudes at their contact points on the other hand. With increasing distance from the fixed edge streamline, elliptical orbital paths result, whose axes perpendicularly to the edge streamline grow at the expense of the axes parallel to the edge streamline.

At the fixed inclined boundaries - as with the above defined negative Clapotis - there are the mentioned linear polarized vibrations of the water particles in the edge streamline. This is due to the fact that here the circular orbital velocities of the incident and mirrored kinematics - according to the continuity condition - are to be superimposed in the same size but with opposite signs.

Examples of the construction of elliptical orbital paths using the graphical vector addition are shown in relation to the configuration of the hydraulic model for the layer depth $d_2 = 0.412$m and for the still water level ($d_0 = 0$m) in Figures 8 and 9 and for inclined embankments in Figures 13 to 16. In addition to the magnitudes of the resulting orbital velocities changing with the position, the shape of the orbital paths can be adjusted quite precisely to the totality of the tangential velocity vectors by means of a drawing program.

For example, for the alternative exact vector addition, the tabular scheme for two consecutive phase points on the orbital circuit is given, which provides the vector inclinations and magnitudes as well as the equations of the ellipse tangents.

The continuity condition is also taken into account by the use of the ERR in that the disappearance (or reduction) of the orbital velocity components normally to the fixed flow boundary is connected with the doubling (or corresponding magnification) of the orbital velocity components parallel to the edge streamline.

Chapters 9 and 10: In order to represent the applicability of the ERR method for the whole range of eligible seabed inclinations between 0^o und 90^o ($0 \leq \alpha \leq 90$), or to distinguish between positive or negative reflection, the subdivision of the regular wave cycle to 16 phase points (with angular distances of 22.5^o) is also used for the tabular vector calculations.

Taking into account the phase difference $\Delta\varphi$, dependent from α, on the one hand and the exponentially reduced mirrored orbital circle diameters on the other, the resulting water level deflections ζ_{res} and the magnitudes W_i of the orbital velocities also can be determined formally by the superimposition of properly phase-shifted cosine functions, see Figures 19 to 23.

Following the concept of the ERR, the resulting water-level deflections $\zeta(d0.i)$ (with $I \leq i \leq IV$) result from the sums of the incoming orbital circle diameters and the exponentially reduced orbital circle diameters shifted by $\Delta\varphi$ .The resulting orbital velocity magnitudes W(d0.i) are calculated from the component sums of the incoming and phase-shifted exponentially reduced mirrored velocities.

Chapter 11: The ordinate values obtained here as dimensionless sizes of unit functions are converted into dimension-related wave heights or orbital velocities, see. Tab.2.

https://doi.org/10.24355/dbbs.084-202002031131-0

These represent the basis for the representation of the development of the water level deflections near the intersection IP of the inclined edge stream line with the still water level (SWL) compared to the circular incoming wave of the constant height = 0.3m, see Figures 25 and 26.

Thus, the maximum water level deflections ζ_{res} with wave heights $H \geq H(circ)$ at inclinations $\alpha \geq 45^o$ can be attributed to the positive reflection and at lower inclinations with the wave height $H < H(circ)$ to the negative reflection.

Another notable result is that the positions of the oscillation nodes for inclinations $0^o < \alpha < 90^o$ appear to deviate so from the still water level that in the vibration cycle they are in pairs both horizontally and vertically dependent on the predetermined inclined edge streamline, see Table 3 and Fig. 24. In particular, from the sequence of functions ζ_{res} with respect to the 5 from slope $\alpha = 90^o$ (Fig.19) to $\alpha = 90^o$ decreasing inclinations (Fig.23) the successive displacement by each $\Delta\beta = 22.5^o$ of the vibration antinodes and the nodes can be observed.

Chapter 12: Finally, the essential result of the dependence of the phase shift between incident and reflected regular cosine waves from the seabed inclination and the resulting interference is summarized in pointer diagrams for the CRC.

The striking result is:

For smooth slopes, *theoretical complex reflection coefficients* arise, which depend on the preselected slope inclination only.

The inclination of the slope studied in the model $\alpha = 26.57°$, corresponding to phase shift $\Delta\varphi = 126{,}87°$ occurs together with the magnitude $C_r = 1 \cdot \cos \Delta\varphi = 1 \cos 126.87° = -0.60$.

Thus, the complex reflection coefficient CRC can be considered not only for the inclination of locally existing reflection objects, but in addition to the linear wave theory globally with regard to the ground contact depending on the sea bottom inclination:

$$\Gamma = C_r e^{i\Delta\varphi} = C_r e^{i(180^0 - 2\alpha)} = C_r e^{i180^0} e^{-i2\alpha}$$

$$= C_r(\cos\pi + i\sin\pi) \cdot e^{-i2\alpha} = -C_r \cdot e^{-i2\alpha} = \frac{-C_r}{e^{i2\alpha}}$$

2. Introduction

The role of reflection in surf research.

The phenomenon of reflection of coastal ocean waves had been largely ignored in the analysis of natural and laboratory studies, especially with regard to the breaking of waves on shallow beaches for more than a third of a century. One reason for this may have been the fact that only the idea of positive reflection existed in water waves, especially since the wave theories dating back to the 19th century (according to Gerstner, Airy/Laplace, Stokes, etc.) did not contain any further approaches to this. As a symptomatic for such a limited view, it should be mentioned that both in the author's dissertation in 1974 "On orbital velocities of irregular surf waves" [4], as well as in the previous relevant studies of about 30 authors analyzed therein, the term "reflection" could hardly be found, [4].

https://doi.org/10.24355/dbbs.084-202002031131-0

Nevertheless, the attentive observer was able to perceive the phenomenon of reflection in different forms visually even on flat sloping sandy beaches. However, Shoemaker and Thijsse (1949) [5] had already given an indication of suspected phase shifts.

Only after the author's finding of the alternative of the “partial negative reflection", (Büsching,2010), which additionally occurs when taking into account a phase shift $\Delta\varphi$ (phase jump) between the incident and reflected wave, did it become plausible why, for example, the frequently measured, approximately ground-parallel horizontal orbital velocities during wave breaking could not lead to sufficiently satisfactory explanations.

However, if breaking waves are assigned to the oscillation anti node of an imperfect negative Clapotis with an imperfect node near the impact point of the slope by the still water level (IP), their streamline image may tend to be very in line with the kinematics in the oscillation anti node of partially standing waves.

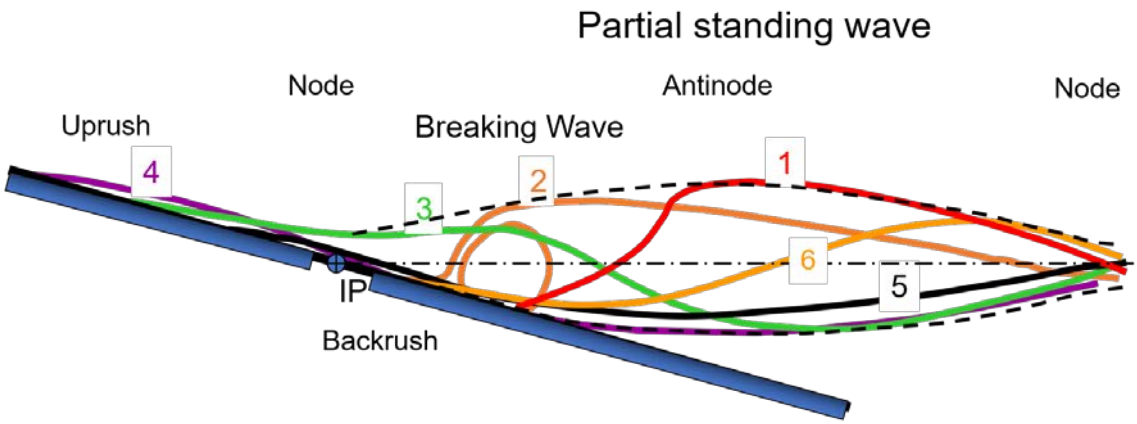

Fig.1: Phases of a breaking wave (plunging / surging breaker) at a phase jump due to partial negative reflection on a slope: In phases 3 and 4, opposite water level deflections take place on both sides of the imperfect Clapotis node, which coincides with IP, approximately. In the theoretical case of negative total reflection, the washing motion can be approximated as a linearly polarized oscillation around point IP.

In order to make the difference between positive and negative reflection clear, the theoretical vibrational forms of a basin with different lateral boundaries with respect to the longitudinal axis, i.e. with on the one hand a vertical wall and on the other hand an inclined wall, are shown in Fig.2. For this purpose, the author has specified the corresponding natural vibration formula as follows:

https://doi.org/10.24355/dbbs.084-202002031131-0

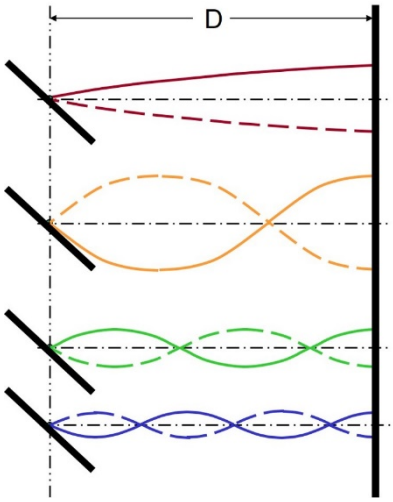

$$f\,[Hz] = (2n+1)\cdot\frac{c}{4\cdot D} \qquad (1)$$

The ordinal numbers n(f) of the vibrations result as follows

$$n(f)[-] = \frac{2\cdot D\cdot f}{c} - 0{,}5 \qquad (2)$$

Fig.2: The first 4 theoretical natural modes of the contents of a basin with a vertical and an inclined wall at distance D.

Thus, with appropriate excitation in a wave channel, both forms of (partially) standing waves can be represented together. While there is an oscillation anti node (of a positive Clapotis) on the vertical wall (possibly also at a wave flap), there is a partial negative Clapotis on the inclined wall (approximate) of the vibration nodes of a partial negative Clapotis. The applicable natural vibration formula is accordingly based on perfectly standing uneven quarter waves [6].

Transferred to the excitation of rope waves, the case shown on the left corresponds to the articulated attachment of the rope to a wall (at IP) and on the right side the case of the free rope end. In nature, on the other hand, either case or the other will occur only, depending on the nature of the reflective structure, i.e. partially standing waves as a result of partially negative or partially positive reflection, unless it is resonance in a basin configuration.

On natural coasts, which are characterized by a dune formation with offshore flat and sandy beach - as is the case with the island of Sylt -both cases are to be distinguished depending on the current water level: At high storm surge water level there is positive reflection from the relatively steep dune embankment, the cliff or the sea wall on the one hand and negative reflection on the other hand at normal water levels from the flat sandy beaches. [7]. In contrast to the model situation of the wave channel, the natural frequency formula (3) is applicable for both expressions in the case of resonance, which is based on perfectly standing half-waves.

$$f\,[Hz] = (n+1)\cdot\frac{c}{2\cdot D} \qquad (3)$$

References to further texts of the author necessary for understanding are given in the relevant context. In particular, it is recommended to have one of the texts [1] or [8].

https://doi.org/10.24355/dbbs.084-202002031131-0

3. Compilation of the symbols and abbreviations used, as well as the characteristic dimensions and parameters relating to the model studies carried out.

α = Slope angle; in the physical model the inclination 1: n = 1:2 ($\alpha = 26.57^o$)
IP =Point of intersection of the slope line and the still water level (SWL).
β = Phase angle in the wave cycle; also measured inclination angle of the long elliptical main axis.
η_{min} , η_{max} = Horizontal distance of the vibration node or of the vibration antinode of (partially) standing waves with reference to IP
$\zeta(\beta)$ = Water level deflection (WLD) as a function of the phase angle β
$\Delta\varphi$ = Phase shift between incoming and reflected (mirrored) wave; phase jump
I , II, III, IIIa and IV = Reflection axes perpendicular to the local ground inclination
d = Layer depth calculated from the still water level (SWL); if necessary with 2 indices separated by a dot.
d0.i = $d_{0.i}$ = Points of intersection of the water level with the axes of reflection I ≤ i ≤ IV.
d3.I = $d_{3.I}$ = 0.626m marks the (constant) depth in the area of the of the flat bottom of the used wave channel, cf. Fif.12
ξ = Mirror depth = vertical distance of the considered wave field point from the intersection of the mirror axis with the edge streamline of the ground. The negative mirror depth ξ' designates the mirrored point beyond the edge streamline of the ground; also breaker index.
$\xi_{0.I}$ = 0.626m = $d_{3.I}$ refers to the depth of the water level above the horizontal channel bottom.
D = Orbital circle diameter
$H_0 = 2\ r_0 = 0.3m = D_0$, nominal partial wave height as a reference value for determined unit wave heights; simultaneously incident wave height of the circularly polarized deep water wave.
$C_r = H_r/H_i$ = Quotient of reflected and incident wave height.
Γ = Complex reflection coefficient (CRC) $\quad \Gamma = C_r e^{i\Delta\varphi}$.
L = 3,8m (2.90m < Li < 4.40m), nominal wavelength representative for i = 5 partial waves from a spectral evaluation, cf. Fig. 11.
T = 1/f = 1.99s (1.684s < Ti < 2.105s) nominal (representative) wave period.
c = L/T = 1,91m/s Phase velocity
W = Orbital velocity magnitude
$W_0 = \pi \cdot D_0/T = 0.47m/s$ corresponding nominal orbital velocity at the SWL as a reference value for determined unit orbital velocities.
circ = Index of parameters of circular orbital motion in deep water

More abbreviations:
ERR = Exponential Reduced Reflection
PC = Positive Clapotis = perfectly standing transverse wave
NC = negative Clapotis = perfectly standing longitudinal wave
WLD = Water level deflection

4. Circular orbital oscillation resulting from two equal frequency, perpendicular oscillations at 90° phase difference.

The following theoretical consideration of the wave movement over a deep sea assumes that the wave field is ideally interspersed with horizontal and vertical vibrational movements of the same frequency. This is prompted by the fact that in the most diverse fields of mechanics the movement on a circle is represented as a circular polarized vibration. This arises in a special case in that two linearly polarized oscillations of the same amplitude and frequency meet perpendicularly with the phase difference of a 1/4 period, i.e. with a phase difference $\Delta\varphi = 90^o$ ($\pi/2$). This may be represented as an interaction of cosine and sinewaves.

https://doi.org/10.24355/dbbs.084-202002031131-0

As is well known, this principle is realized, for example, in the drive of the electric motor, and in its reversal also in the power generator driven by a turbine. Here it is intended to serve as a model for the orbital movement observed in water waves in deep water, such that the latter are regarded as a combination of relatively long-wave longitudinal and transverse waves. It should already be emphasized at this point that phase shifts (phase jumps, phase differences) seem to be able to create an extremely important phenomenon in the interference of vibrations in general, especially in natural processes. Especially since depending on the size of the phase shift also linearly or elliptically polarized vibrational movements (Lissajous figures) can be generated, see below.

With regard to the circular orbital movements of a deep sea, the generator principle is to be considered here for the time being. The disturbance induced by the consequences of wind-generated (horizontal) impulses and gravity action in the form of a circular polarized oscillation is assumed to be the origin of two linearly polarized oscillations perpendicular to each other. Accordingly, on the surface, the progressive waves spreading horizontally and on the other hand, vertically spreading vibrations could arise on the surface. The latter would be subject to an exponentially increasing attenuation with the depth, as these are represented, for example, according to the linear wave theory (Airy–Laplace) in the decrease of the orbital circle diameter according to the known exponential law, cf. Fig. 4.

With the arrangement selected in Fig.3, the circular polarized oscillation (circular oscillation clockwise, red) is created in such a way that the specified phases 1 to 8 are passed synchronously from left to right synchronously with phases 1' to 8' from top to bottom in the specified order. The center of the circle remains also for subsequent wave cycles at the location.

If, conversely, the circular motion is assumed to be the origin (source), the wave forming at the surface would move to the right out of the image, while the vertical linear polarized oscillation would continue below the water level with the exponential damping to the depth of about half a wavelength.

In the following, the orbital movements that result from the water surface (index 0) are mainly considered when both oscillations progress by steps of 1/8 and 1/16 period (T/8 and T/16 respectively).

In contrast to the pictorial representation of wave interferences (especially in the representations of the reflection phenomenon) which are often limited to the water-level deflections ζ, here the vectors of the circumferential velocities $W = \pi \cdot D/T$ are assigned to the wave or oscillation phases respectively. According to this, in the present arrangement in Fig.3 for each resulting vibration phase, the "velocity moment" $M = W \cdot D$, which sets the direction of rotation clockwise.

https://doi.org/10.24355/dbbs.084-202002031131-0

Fig.3: With the chosen arrangement of two vertically polarized vibrations, a circular polarized vibration (circular oscillation clockwise, red) is created. The specified phases 1 to 8 are continuously traversed from left to right synchronously with the phase-shifted phases 1' to 8' from top to bottom in the specified order. The vectors of the circumferential velocities W = πD/T are assigned to the relevant wave phases. According to this, in the present arrangement for each resulting vibration phase, the "velocity moment" M = W·D and the direction of rotation is clockwise.

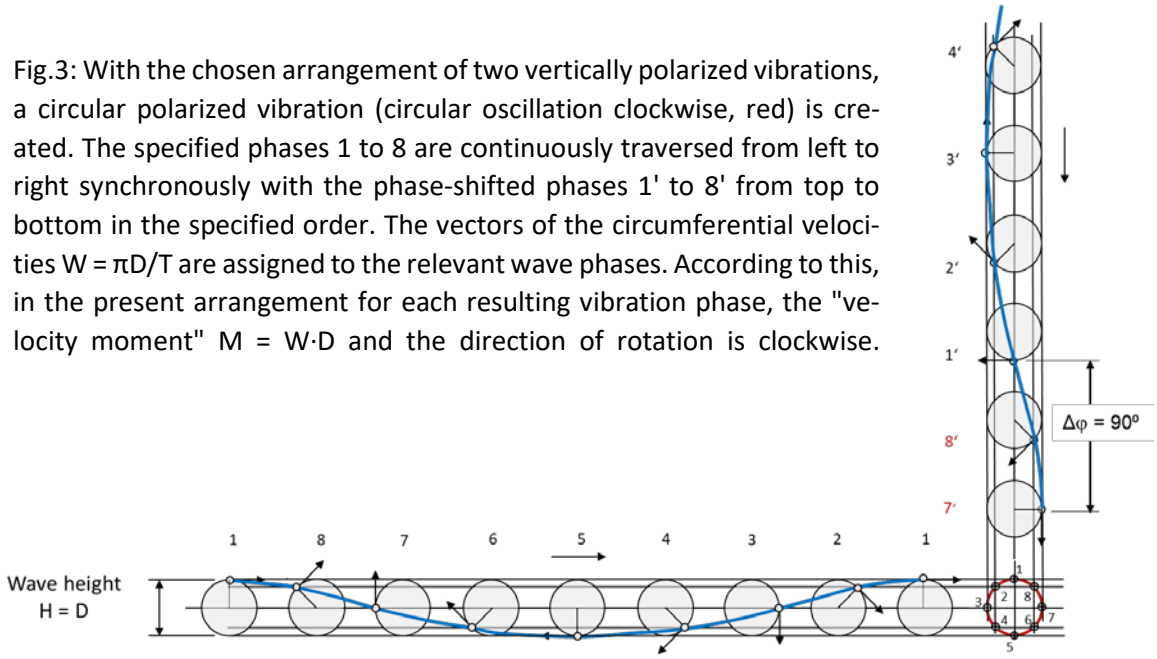

In order to replicate real water waves existing in nature, however, the effect of mass transport would have to be recorded separately taking into account an additional drift current.

On the other hand, asymmetric storm waves in the deep water (on the open sea) could already arise as waves with non-circular orbital movements, if the phase difference between the generating approximately persecuting linearly polarized waves meet with a phase difference of $\Delta\varphi \neq 90^{o}$ ($\pi/2$).

5. Detection of phase jumps in waves in the hydraulic model

Convinced that the known wave theories would hardly be helpful to verify the findings obtained in the wave channel of the FH Bielefeld University of Applied Sciences (specifically for the use of a complex reflection coefficient), relationships with the known theoretical shallow water approaches - besides the decrease of the orbital circle diameter according to the known exponential law – had not been made.

Rather, with regard to the kinematics of water particles in the area of decreasing water depth in the context of this article, the author confines himself to the application of only the basic trigonometric functions in the linear oscillation theory. The aim is to recognize functional connections to the phenomenon of phase shift in reflection found in the model and to present them primarily graphically.

A complete analytical formulation of the intended supplement of linear wave theory should be reserved for a further publication if necessary.

https://doi.org/10.24355/dbbs.084-202002031131-0

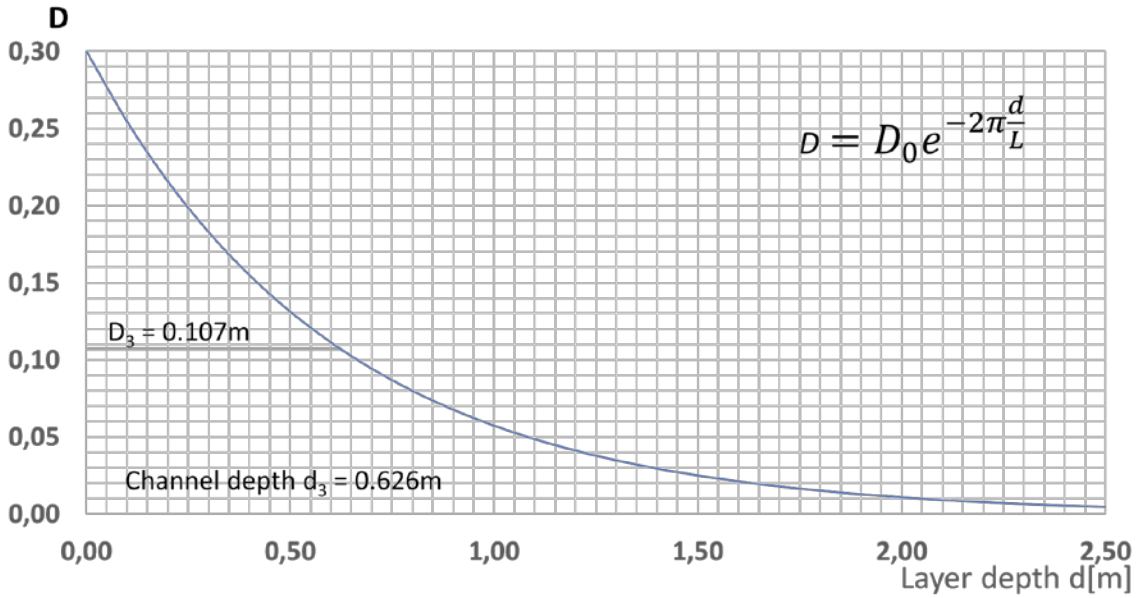

Fig.4: Orbital circle diameter D[m] for water depths in the wave channel above (or below) the channel bottom relative to a nominal wave height H = 0.3m and the wavelength L = 3.8m, which come from the results of the relevant model studies, see. Fig. 5.

Instead of the progressive pressure changes, the focus here should be on the consideration of the orbital movements changing in the wave field from circular to elliptical.

Adapted to the range of model dimensions, the orbital diameters D according to the relationship

$$D = D_0 e^{-2\pi\frac{d}{L}} \quad (4)$$

can be taken from Fig.4.

In the theoretical treatment, particular reference is made to the real dimensions of the relevant model configuration, see Fig. 5.

The corresponding graph with reference to the geometry of the model configuration in the wave channel used contains Fig. 5.

https://doi.org/10.24355/dbbs.084-202002031131-0

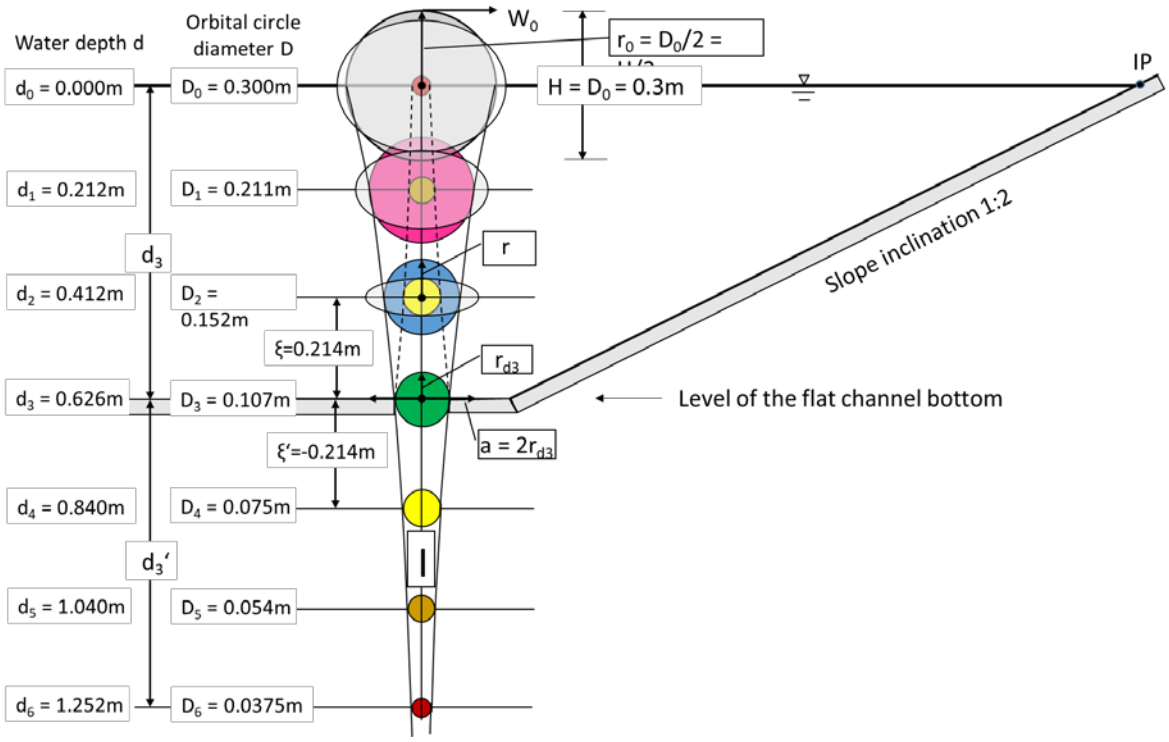

Fig. 5: Design of the elliptical orbital paths at water depths d < L/2 by superimposing the reflected kinematics of a deep sea in the positive mirror depth range of 0.626m according to the analytical formulation with reference to Schulejkin (1956). Further explanations, in particular in Chapter 6.

The relatively small maximum water depth d_3 = 0.626m << L/2 is known to cause deformations of the orbital paths, the extent of which affects not only the close range of the flow, but the entire flow field. Of essential importance is the respective shape of the fixed edges of the wave field, since no vertical movements are possible for these.

Existing nonlinear theories for wave movement in the range of decreasing water depths have often been tested for their applicability with only moderate success. This applies in particular to the description of the flow processes in (relatively small-scale) wave channels. The author, however, tried to provide a clear interpretation of the basic physical processes.

The approximately spiral orbital motion, which can be generated by a superimposed drift current, on the one hand, the wave breaking on the other hand and other wave-deforming "compression effects" observed in the wave channel and resulting nonlinearities are not addressed [8] here.

https://doi.org/10.24355/dbbs.084-202002031131-0

6. Importance of boundaries for kinematics in orbital velocity field

The most striking practical example of the reflection of water waves is the kinematics of the incoming and reflected waves on an ideally smooth vertical wall, see Fig.6.

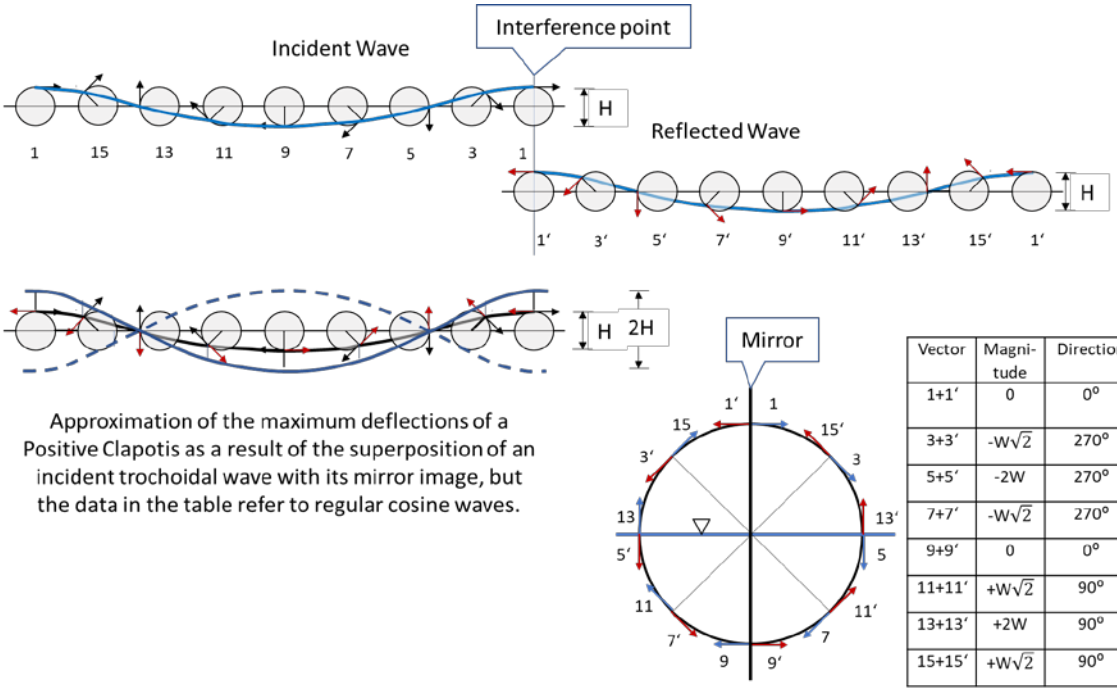

Vector	Magni-tude	Direction	WLD
1+1′	0	0°	+2*H/2=+H
3+3′	-W$\sqrt{2}$	270°	$+H\sqrt{2}/2$
5+5′	-2W	270°	0
7+7′	-W$\sqrt{2}$	270°	$-H\sqrt{2}/2$
9+9′	0	0°	-2*H/2=-H
11+11′	+W$\sqrt{2}$	90°	$-H\sqrt{2}/2$
13+13′	+2W	90°	0
15+15′	+W$\sqrt{2}$	90°	$+H\sqrt{2}/2$

Fig.6: The water level deflections of two counter-rotating regular cosine waves are shown. The orbital vectors are assigned to the orbital vectors according to direction and magnitude. The horizontal reflection without phase jump ($\Delta\varphi = 0°$)results in a vertical linearly polarized oscillation of the water particles, for example on a vertical wall (mirror).

If a progressive wave train hits such a wall, a mirror-image wave train is thrown back by it. It is well known that the superimposition of incident and reflected waves produces a standing wave, which is classified as positive Clapotis according to the above definition. This is the result of two equally interconnecting waves without the appearance of a phase jump between them, as wave crests are reflected by wave crests and wave troughs through wave troughs.($\Delta\varphi = 0°$) This fact applies again not only to the water particle movement at the water surface in relation to the still water level (SWL) but in a similar way also in relation to the layer depths lying below with the associated orbital circuit decreasing according to the specified exponential law with the water depth, see Fig.4.

With regard to the resulting orbital velocities, it is of particular importance in the reflection that the orbital movements of the incoming and the reflected waves have an opposite sense of rotation. In the case of the circular orbital motion, the velocities of the reflected wave at the point of reflection (interference point) are equal to those of the incoming orbital motion. As a result, when both are superimposed, their horizontal components are removed, while the mirror-parallel vertical components double. That is, on the vertical wall as well as in all Clapotis antinodes (loops) the vector addition of the originally circular movements of the incoming and the reflected wave for a wave cycle results in the vertical linearly polarized oscillation of a transverse wave with maxima ±2W_0. Conversely, at the vibration nodes, the horizontal speed components reach their maxima at the

https://doi.org/10.24355/dbbs.084-202002031131-0

expense of the vertical components with a value of ±2W0 Conversely, at the vibration nodes, the horizontal speed components reach their maxima at the expense of the vertical components with a value of $\pm 2W_0$.

W_0 is the circumferential velocity of the water particles on the orbital circle at the water surface of a deep sea according to $W_0 = \pi D_0/T$ with a diameter D_0 equal to the wave height H relative to the wave period T.

This unit value W_0 can be assigned for the surface of each considered wave phase, and it is also considered a reference value for the lower (exponentially reduced) velocities at the layer depths below. For the interference studies carried out here, bases for the orbital velocity vector were selected on the orbital circuit, depending on the accuracy requirement per wave cycle 8 or 16, regularly distributed on the circumference.

Provided that the orbital movements of a deep sea at a layer depth less than half the wavelength are synchronous with those on the surface, the simultaneous observation of two circular orbital paths in different layer depths i and n, the relationship between the magnitudes of the velocity vectors concerned are as follows:

$$\frac{W_i}{W_n} = \frac{\pi \cdot D_i}{T} \cdot \frac{T}{\pi \cdot D_n} = \frac{D_i}{D_n} \qquad (5)$$

That means that the circumferential velocities W behave like the orbital path diameter D, where $n \neq i$.

Thus, for the time being, no concrete values for wave height H and period T are required. Rather, unit-circle observations at the orbital circles of the water surface are sufficient to determine the velocities resulting from the vector addition according to magnitude and direction as well as the associated resulting water level deflections ζ. The same applies to the layer depths positioned below the water surface.

For the successive overlay phases 1+1', 3+3', 5+5', 7+7', ... the respective velocity resulting from the vector addition by magnitude and direction can be determined at the respective orbital circle (unit circle with the radius H/2) for the interference point, cf. Table in Figure 6.

In the Clapotis phases, in which the maximum positive or negative water level deflections double (phases 1+1' and 9+9'), the sign change of the vertical vibration direction of the water particles takes place. That is, the current orbital velocities of the opposing waves cancel each other's entire wave field. In the following vibration phases, especially in the oscillation loops of the Clapotis (as well as at the interference point (position of the vertical wall), only the horizontal components of the orbital vectors cancel each other, so that the positive Clapotis on a wall gets the character of a transversal wave. The maximum vertical orbital velocities when swinging through the still water level are $\pm 2W_0$ (phases 5+5' and 13+13').

Since the vertical components in (and below) the oscillation nodes cancel each other, the horizontal oscillation movements there theoretically also reach their maximum values of $\pm 2W_0$. The corresponding swinging directions (directions of the streamlines of the positive Clapotis) run accordingly perpendicular to the shown velocity vectors canceling each other.

https://doi.org/10.24355/dbbs.084-202002031131-0

Theoretical negative Clapotis

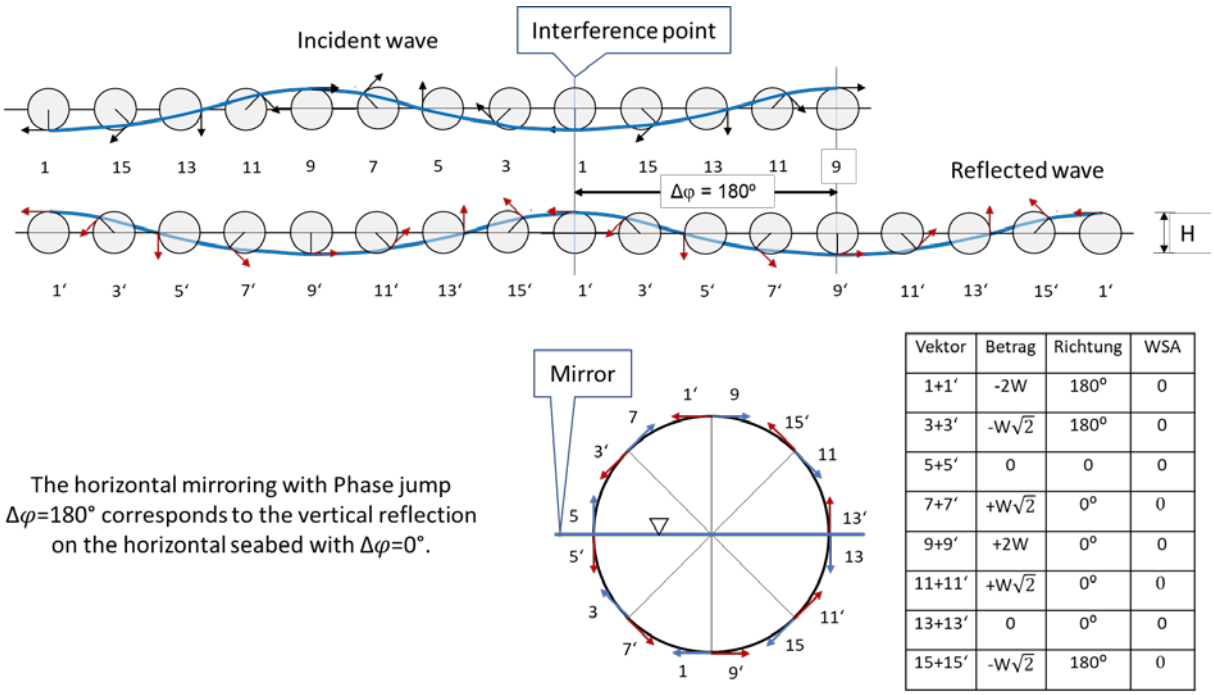

Vektor	Betrag	Richtung	WSA
1+1'	-2W	180°	0
3+3'	$-W\sqrt{2}$	180°	0
5+5'	0	0	0
7+7'	$+W\sqrt{2}$	0°	0
9+9'	+2W	0°	0
11+11'	$+W\sqrt{2}$	0°	0
13+13'	0	0°	0
15+15'	$-W\sqrt{2}$	180°	0

Fig.7: On the horizontal seabed, the horizontal reflection (mirroring) at the phase jump of $\Delta\varphi = 180°$ corresponds to vertical reflection at the ground (or water level) with the phase difference $\Delta\varphi = 0°$, see also Fig. 16.

In contrast to the positive Clapotis (PC), the author uses the term "negative Clapotis" (NC) for a vibration in which the phase jump (phase difference) between the incoming wave and the reflected wave is $\Delta\varphi = 180°$. In this case, wave crests would in principle be reflected through wave troughs and vice versa. Such a configuration is only theoretically conceivable, in the event that the (fictitious) kinematics of a deep sea on the (horizontal) seabed of a shallow sea is reflected exponentially reduced. Such a study was carried out by Schulejkin (cf. [2] and Chapter 6). But he did not consider a link with the phenomenon of a phase difference of interfering waves. In fact, there is no complete extinction of water level deflections on the surface. Rather, the theoretical term refers to the seabed, which is conceived as a mirror, on which similar kinematic processes take place as described above for the reflection on the vertical wall. As already shown in Fig.5 in relation to the flat ground of the wave channel, there is also the superimposition of two orbital circles of the same size with opposite sense of rotation. As a result, in this boundary case, the standing wave appears as a horizontal linearly polarized oscillation motion at the bottom of a shallow sea, in the sense of a longitudinal oscillation, which, for example, changes in pressure in sound waves (compression and dilutions of the molecular distances).

If the construction of the resulting orbital velocities is carried out according to the same principle as for the positive Clapotis by horizontal reflection on a vertical mirror, however, in relation to the horizontal seabed (in the model for water depth d_3), the vector additions for the successive overlay phases 1+1', 3+3', 5+5', 7+7' ... by magnitude and direction are again tracked at the orbital circle (unit circle) shown with respect to the present water depth, cf. Table in Fig.7.

https://doi.org/10.24355/dbbs.084-202002031131-0

In the Clapotis phases, in which the maximum amounts of the water level deflections are reduced to zero (1+1' and 9+9'), the vertical components of the current circumferential velocities cancel each other according to the continuity condition, with the result that the horizontal components reach their maximum positive or maximum negative magnitude of ± $2W_3$. In the intervening phases, the magnitude zero is gradually reached in each of the reverse points.

7. Orbital movement in a shallow sea

In order to illustrate the change in the kinematics of the wave field in the consideration of the bottom in a more illustrative and physically comprehensible way, Schulejkin (1956) deviated from the usual mathematical derivation of the water particle movement and instead also uses a method of mirroring [2]. Thus, the orbital motion can be constructed with ground contact from that of the one without ground contact (of a deep sea). For this purpose, the ground is understood in a depth $d < L/2$ as a mirror in such a way that the orbital kinematics, which continues exponentially reduced behind the mirror according to equation (4), superimposes the orbital kinematics that initially exist in front of the mirror.

For this purpose, Schulejkin had derived mathematically the algebraic formulations of the horizontal and vertical orbital coordinates of the orbital velocities for water particles on elliptical orbits in a shallow sea, however related to the boundary condition of the horizontal flat ground only.

The author subsequently extends the application of this method in such a way that he also adapts it to horizontally deviating flow boundary (inclined seabed, especially flat embankments). At the same time, the orbital velocities of partially standing waves are determined by magnitude and direction using the graphical or computational vector addition. The input data is based on the model dimensions used in the own model studies. In order to make the results comparable with the model studies, these are taken into account in Figs. 5 and 12 on a scale basis.

The geometry shown there is accordingly oriented to the configuration and results of the laboratory tests for a smooth revetment of inclination 1: n = 1: 2 in the wave channel, whose water depth was d = 0.626m. Thus, the length L = 3.8m of the partial wave of the partial frequency range $0.4875\text{Hz} \leq f \leq 0.51875\text{Hz}$ was examined in more detail, see. Büsching (2011) [1], and Fig.11.

Since the studies in question are based on the analysis of the energy values of partially standing waves (instead of measuring the heights of incoming and reflected waves), the wave height parameter H = D = 0.3m used below, does not represent a measured value, but is to be regarded only as an exemplary input value H_i of a wave coming in from the deep water.

A prerequisite for the graphical-computational representation or determination of the orbital movements in the area at and above the flat channel bottom (in Fig.5) is the choice of suitable scales for the geometry and the orbital velocity.

According to the reflection concept, the horizontal bottom of the wave channel (seabed) is initially considered non-existent and the orbital movements of a deep sea decreasing with the depth are present according to equation (4), cf. Fig.5.

According to this, for the positive local coordinate ξ_i emanating from the ground, the water particles would move around the center of a circle with the corresponding radius r_i

https://doi.org/10.24355/dbbs.084-202002031131-0

Here, the orbital motion is represented analogously to the above observation of 8 wave phases by each at 8 evenly distributed on the circumference orbital vectors W_i of equal amount.

The same would apply in turn to the movement of water particles at the level of the bottom and below.

When mirroring the circular orbital movements present at a distance -ξ under the ground, these are to be superimposed on the corresponding circular orbital movements above the ground at a distance of +ξ, but with the opposite sense of rotation.

As a result, for each layer depth above the ground, the resulting orbital path is obtained as an ellipse, the long horizontal half-axis of which is equal to the sum of the radii of the generating orbital circles (in the deep sea) and whose short half axis is determined by the difference of the two radii in question.

Thus, for a shallow sea with flat ground, one can say that the effect of the boundary condition, usually referred to as "bottom contact", can be characterized more clearly and precisely as a reflection effect of the seabed. The mirrored orbital velocities to be superimposed only enter at a fraction of the incoming local orbital velocities, depending on the respective mirror distance.

In addition, the continuity condition is taken into account here in that the disappearance of the vertical oscillation movement at the ground comes with the doubling of the horizontal oscillation on the ground (or in the inclined edge streamline).

The author has chosen the shortening term "exponentially reduced reflection (mirroring)" for this procedure and uses the abbreviation ERR.

In the case of the regular cosine-waves provided here, the resulting magnitude of the velocity $W_{r,i}$ (for the respective layer depth i) changes continuously during the particle movement on an ellipse.

At the water surface, the maximum velocities are assigned to the wave crest or the wave trough, while the minimum velocities are vertically oriented and relate to the phases of the intersection of the wave profile with the reference horizon (still water level respectively). The same applies correspondingly reduced for the layer depths below.

Because of the exponentially decreasing orbital circle diameters with the water depth, for the investigations of the flow field advantageous layer depths with equal distances should be chosen. In the present case, however, this is partially realized only in approximation.

In the following, the graphically vector addition is shown as an example for the layer depth d_2, for the water level d_0 and for the channel floor d_3, cf. Fig.5.

For the distinction from the 4 inclined mirror axes II, III, IIIa and IV examined below at the inclined slope level, see Fig.12, the configuration with vertical mirror axis in Fig. 5 was designated with Roman I.

The reference to this, as well as to the other mirror axes mentioned above, is given separately by a dot for the water depths in the index concerned.

For the layer depth $d_{2.I}$ = 0.412m (corresponding to the coordinate ξ = 0.214m), the graphic construction of the orbital path and the resulting orbital vectors corresponding to the position on this changing orbital pathway can be taken from Fig. 8.

https://doi.org/10.24355/dbbs.084-202002031131-0

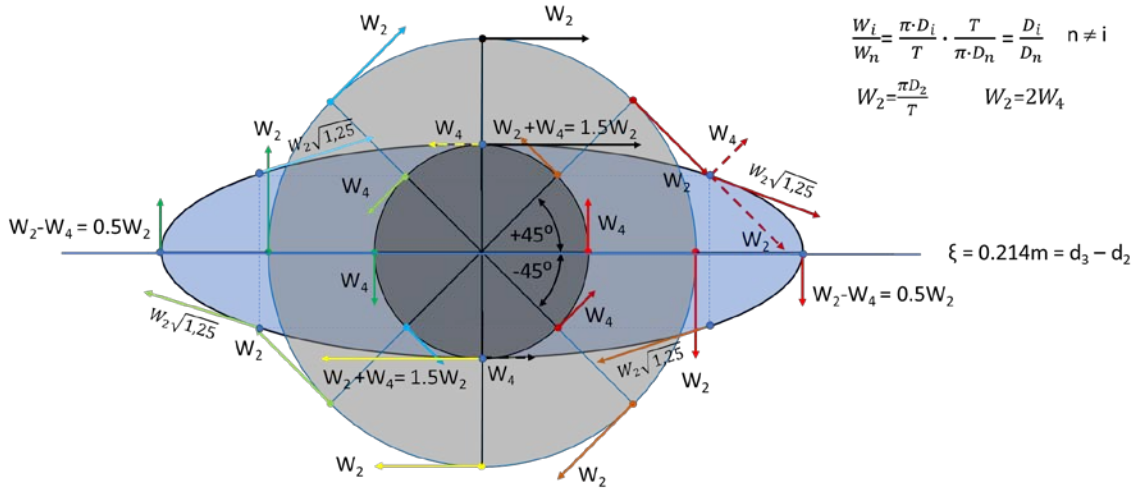

Fig. 8: Graphic determination of the elliptical orbital path for a shallow sea. Mirror axis of configuration I. Special case of vector addition for the ratio $D_{2.I}/D_{4.I} = 2/1$, which results for the layer depth $d_{2.I} = 0.412$m according to the coordinate $\xi = 0.214$m and the exponentially reduced reflection (ERR) of the orbital motion at $\xi = -0.214$m (below the ground). Thus, the relationship $W_2 = 2W_4$ applies to the circumferential velocities.

Again, in this case, the resulting values for the maximum and minimum orbital velocity vectors are given depending on the local circular circumferential velocity. In addition, the graphical vector addition of the vectors W_2 and W_4 (dark red) is shown for the horizontal phase angles $\Theta = +45^{o}$ and. $\Theta = -45^{o}$, the resulting value of which indicates the magnitude and direction of the tangent to the resulting ellipse. The reference points for the other resulting velocity vectors (brown, light green, blue) at the sought ellipse are also found by mathematical-graphical vector additions or by symmetry considerations, so that the elliptical orbital path can be entered into the velocity vector plan with great accuracy.

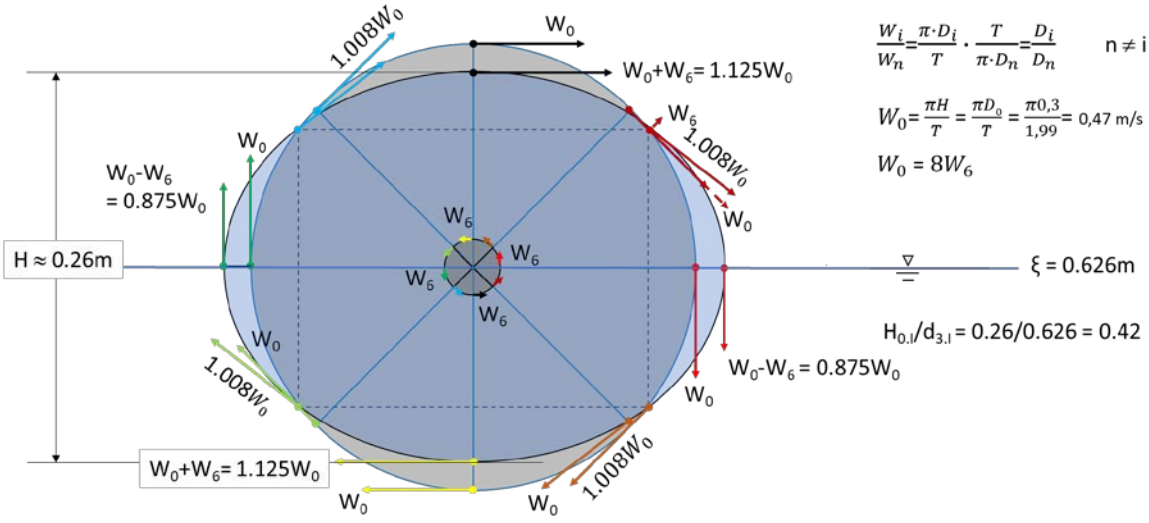

Fig.09: Graphic determination of the elliptical orbital path for a shallow sea with flat ground. Mirror axis of configuration I. Vector addition for the ratio $D_{0.I}/D_{6.I} = 0.3\text{m}/0.0375\text{m} = 8/1$, which results for the still water level according to the coordinate $\xi = d_{0.I} = 0.626$m and the reflection of the orbital motion at $\xi = -0.626$m (below the ground), cf. Fig. 5.
Thus, the relationship $W_0 = 8W_6$ applies to the circumferential velocities.

https://doi.org/10.24355/dbbs.084-202002031131-0

As a special case according to the boundary condition on the bottom, once again the horizontal linear polarized oscillation results from the superimposition of two equal orbital circles but opposite circumferential velocities.

Their maximum velocities can in turn be indicated with the 2-fold amount of the generating circular movements on the ground depending on W_3 with $2W_{3,}$, cf. Fig.7. The absolute amounts for this purpose, as also those for the following remaining layer depths of the mirror axis I with the indices 2, 1 and 0, are to be found in Table 1.

The graphical-computational vector additions of the two circular opposite orbital velocities in Figs. 8 and 9 thus provide not only the elliptical orbital curves but also the magnitudes of the resulting orbital velocities. The shape of the trajectories could be adjusted very precisely to the totality of the tangential velocity vectors by means of a drawing program.

In contrast to the method of the ellipse construction according to Phillipe de la Hire, which is based on the use of the two vertex circles, the generating orbital circuits are used here for the representation of the elliptical orbital path in such a way that the long horizontal half-axis consists of the sum of the radii of both orbital circles and the short vertical half-axis b results from the difference of the latter.

With regard to the extreme values of the orbital velocities, the following applies:

The maximum (horizontal) orbital velocities on the ellipse are the sum of the circular orbital velocities involved and the minimum (vertical) orbital velocities result from their difference.

Alternatively, the parameter representation for the ellipse curve is:

$$\begin{pmatrix} x = a\ \cos t \\ y = b\ \sin t \end{pmatrix} \text{ with } 0 \leq t \leq 2\pi \qquad (6)$$

and for the linearly polarized particle oscillation at the horizontal bottom at depth d_3 is a = r, so that

$$\begin{pmatrix} x = 2r_3 \cos t \\ y = 0 \end{pmatrix} \text{ with } 0 \leq t \leq 2\pi \qquad (7)$$

8. Phase shift at an inclined plane

Since the linearly polarized vibrations at the fixed flow edges had represented the appropriate boundary condition both for the appearance of the positive Clapotis (with $\Delta\varphi = 0^o$) on the vertical wall and for the negative Clapotis on the horizontal ground (with $\Delta\varphi = 180^o$), the conclusion is inevitable that such vibrations also occur on inclined flat surfaces.

The linear relationship in question between the phase shift $\Delta\varphi$ and the slope, is then:

$$\Delta\varphi = 180° - 2\alpha \qquad (8a)$$

respectively

$$\alpha = 90° - 0.5\Delta\varphi \qquad (8b)$$

Thus, for the slope 1:n = 1:2 corresponding to 26.57^o, the associated phase shift between the incident and the reflected wave is

$$\Delta\varphi_{theo} = 126.86°$$

cf. Fig.10.

https://doi.org/10.24355/dbbs.084-202002031131-0

In fact, this value of the phase shift is almost exactly the same as that found by the author in [1] for the reference wave specified here and there at a slope 1: 2. Therefore the phenomenon of the phase shift as a component of the Complex Reflection Coefficients (CRC) can now also be regarded as theoretically verified. The pictorial representation characteristic of this situation is here Fig. 11.

It should be mentioned that the energy values shown for partially standing partial waves also document the horizontal wave asymmetry occurring with approach to the embankment structure.

For this reason, in the present case, the phase shift of two measured values is defined such that their mean value is

$$\Delta\varphi = \frac{132.6°+123.2°}{2} = 127.9° \approx 126.86° \qquad (9)$$

If, alternatively all 5 partial waves of the spectral core range considered in (Büsching, 2011) and (Büsching, 2012) are taken into account in the same way, the arithmetic mean is obtained for this purpose:

$$\Delta\varphi = 132.00^0 \approx 126.86° .$$

It should be noted that the (small) deviation from the former can be explained not only from the relative displacements of the 5 partial waves to each other and the frequency-dependent compressions documented in Fig. 11, but also rounding errors specifically in the determination of the lengths of the partial waves may be mentioned.

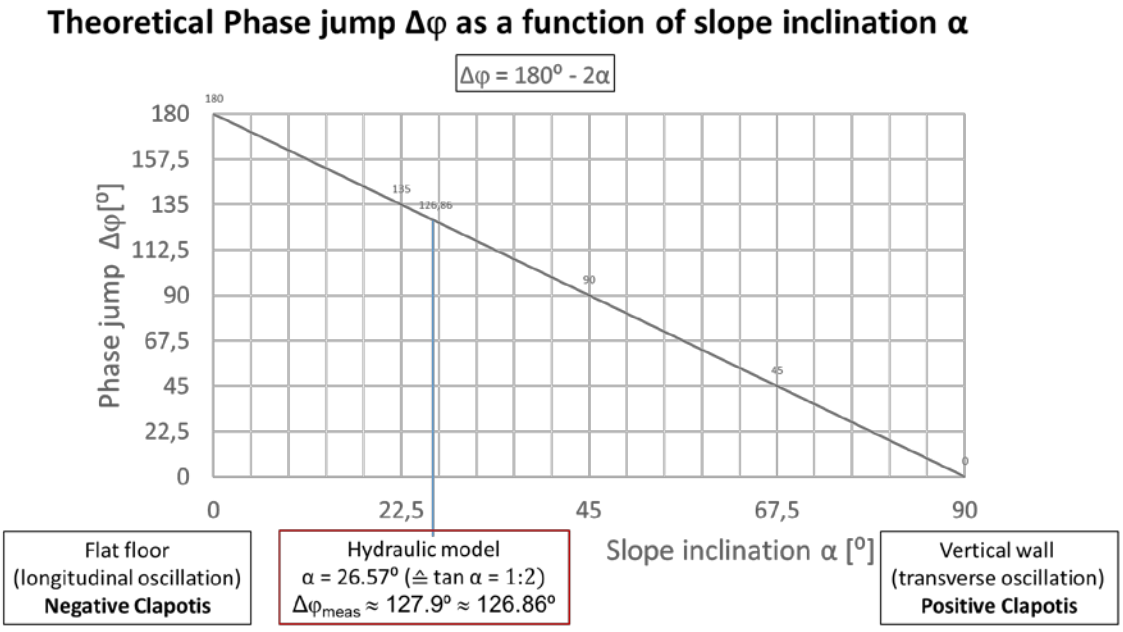

Fig.10: Phase jump $\Delta\varphi[^0]$ between incident and reflected wave as a linear function of the slope angle $\alpha[^0]$.

https://doi.org/10.24355/dbbs.084-202002031131-0

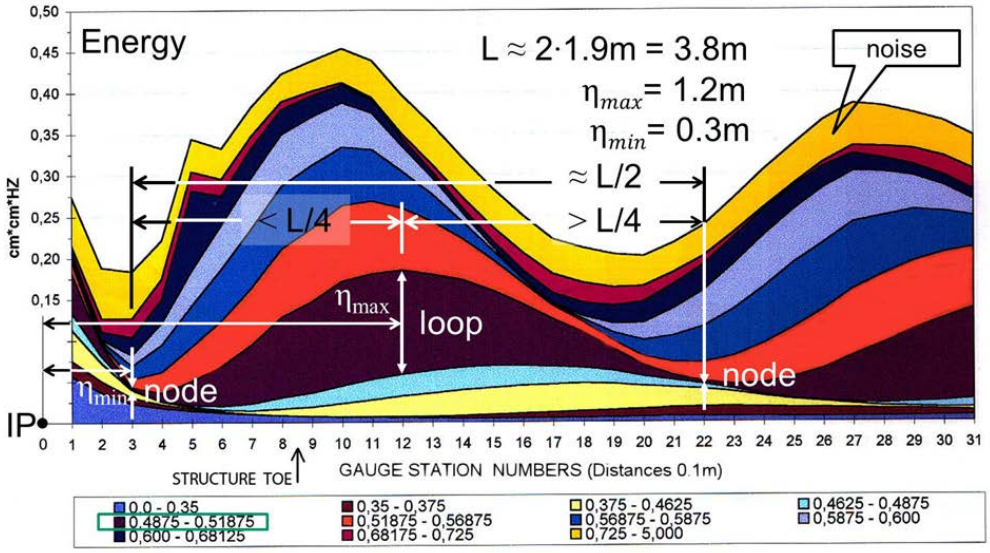

Fig.11: To determine the length L and the phase difference Δφ between incident and reflected wave using the example of the partial wave of the frequency range $0.4875\text{Hz} \le f \le 0.51875\text{Hz}$ at a flat slope 1:2. As a result of the horizontal wave asymmetry of the almost breaking waves (characterized by $\eta_{max} - \eta_{min} < L/4$), the formulas (10a) and (10b) provide two different results for the phase shift $\Delta\varphi = 132.6^0 > 123.2^0$.
Further explanation in (Büsching, F., 2012 [1]) or (Büsching, F., 2011 [8]).

According to the author's research, the phase shift can be obtained from the application of the energy values calculated above the distance of IP, using spectrum analysis. To do this, the distances of the IP-nearest energy maximum (characterized by an imperfect oscillation loop) η_{max} and the adjacent energy minimum (characterized by an imperfect vibration node) η_{min}, have to be measured in Fig.11. The approximate phase difference then results from the mean of the formulas (10a) and (10b):

$$\Delta\varphi[^\circ] = 360\left(1 - \frac{2\,\eta_{max}}{L}\right) \qquad (10a)$$

$$\Delta\varphi[^\circ] = 180\left(1 - \frac{4\,\eta_{min}}{L}\right) \qquad (10b)$$

Since the phase shift parameter $\Delta\varphi$ according to equation (8a) contains that of the ground inclination α, the complex reflection coefficient (CRC) can now also be regarded as a transformation parameter for waves over decreasing water depth.
Together with the inland shift of higher frequency energy components (short-waves) compared to lower-frequency components (longer-waves) documented in Fig. 11, this could in future also provide the basis for a paradigm shift in the treatment of the wave deformation in the area of decreasing water depth. For now, profile deformations of waves at changing inclination angles of the seabed in the surf area can theoretically (and vividly) also be attributed to vibration interferences.
In particular, higher-order approaches to describe wave deformation should also be reviewed with regard to the use of the Phase Shift parameter.

https://doi.org/10.24355/dbbs.084-202002031131-0

9. Graphical and mathematically accurate addition of orbital velocity vectors with respect to slope 1: 2.

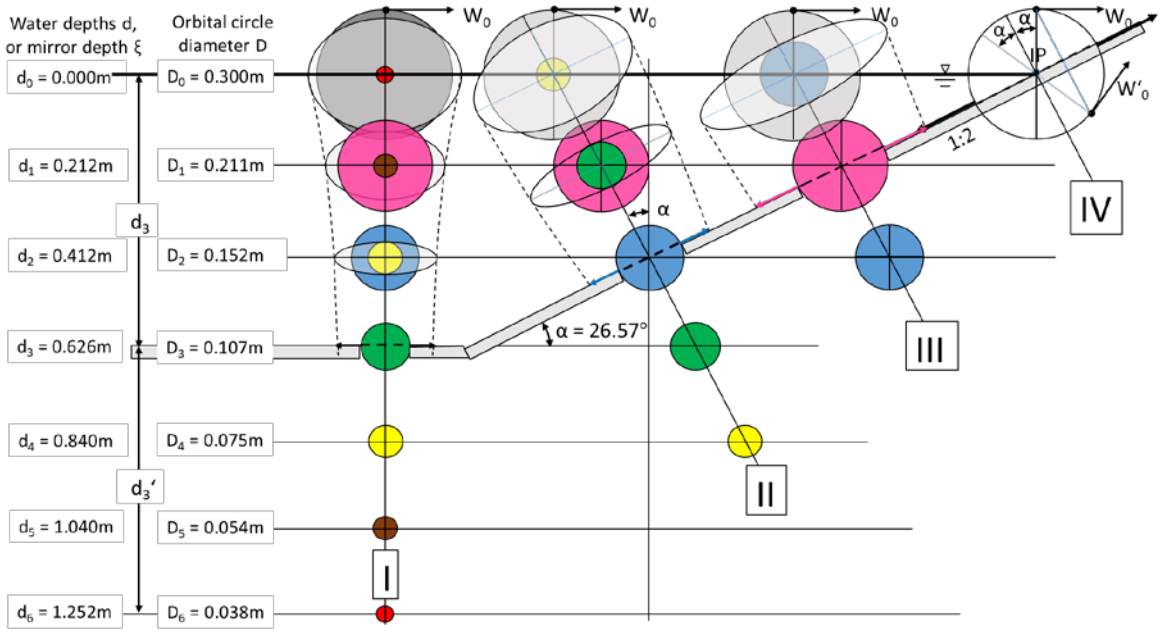

Fig.12: Overview of elliptical orbital movements in the area of limited water depth using the example of a smooth slope inclined 1: n = 1: 2 in the wave channel. The results for investigations on the mirror axis I to IV are shown. Calculations with regard to an additionally included mirror axis IIIa between axes III and IV are not taken into account here for drawing reasons. Explanations of the method of superimposition used in the "exponentially reduced reflection" of orbital kinematics are given below.

The basic input data, for the rotated elliptical orbital paths in Fig. 12, are shown in the illustrations in Figures 13 to 16. In each case, the underlying vector plan is shown with respect to the orbital velocity vectors to be superimposed. Accordingly, 8 phase points (with angular distances of 45°) on the orbital circles for the circular orbital velocity were assumed here, wherein the same color was chosen for the respective velocity vectors to be added respectively. Ordinal numbers of exponentially reduced mirrored vectors are provided with apostrophe.
The vector additions were also carried out here with the help of a drawing program both graphically and mathematically. Figures 13 to 15 show the graphical determination of the resulting vector by magnitude and direction in each case at the top right of the vector pair 1 + 1'.

https://doi.org/10.24355/dbbs.084-202002031131-0

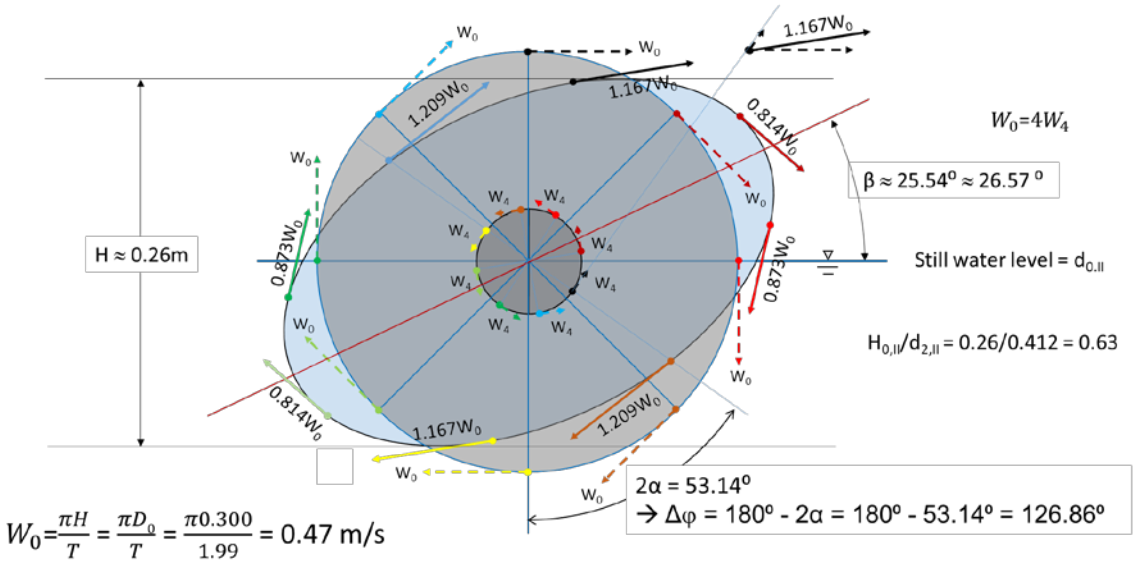

Fig. 13: Graphical determination of the elliptical orbital paths above the slope 1: n = 1: 2, (corresponding to $\alpha = 26.57^0$). Mirror axis of configuration II. Vector addition for the ratio $D_{0.II}/D_{4.II} = 0{,}300m/0{,}075m = 4$, which results in the water level ($d_{0.II} = 0.0m$) corresponding to the coordinate $\xi = 0.412m$ and the reflection of the orbital motion at $\xi' = -0.412m$ (below the inclined ground), cf. Fig.12. Thus, the relationship $W_0 = 4W_4$ applies to the circumferential velocities on the elliptical path.

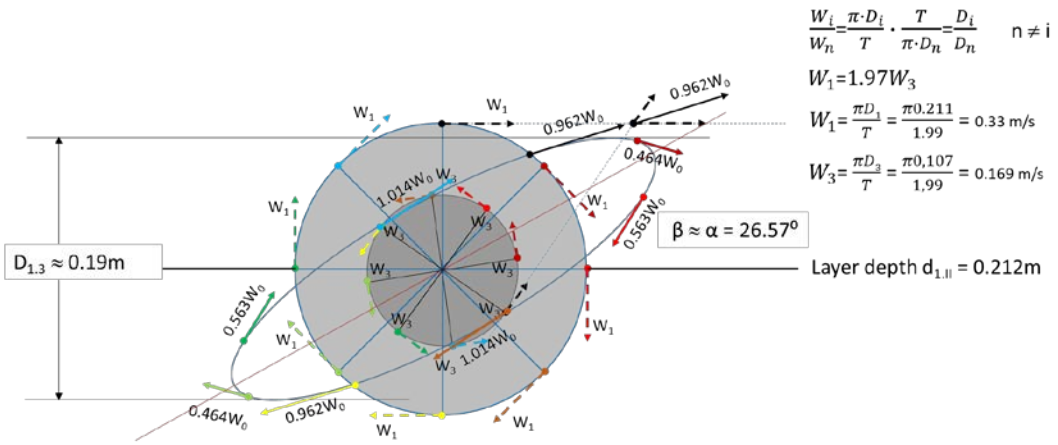

Fig.14: Graphical determination of the elliptical orbital paths above the slope 1: n = 1: 2, (corresponding to $\alpha = 26.57^0$). Mirror axis of configuration II. Vector addition for the ratio D1/D3= 0.211m/0.107m = 1.97, which results in the water level ($d_{1.II} = 0.212m$) corresponding to the coordinate $\xi = 0.2m$ and the reflection of the orbital motion at $\xi' = -0.214m$ (below the inclined ground), cf. Fig.12. Thus, the relationship $W_0 = 4W_4$ applies to the circumferential velocities
on the elliptical path.

https://doi.org/10.24355/dbbs.084-202002031131-0

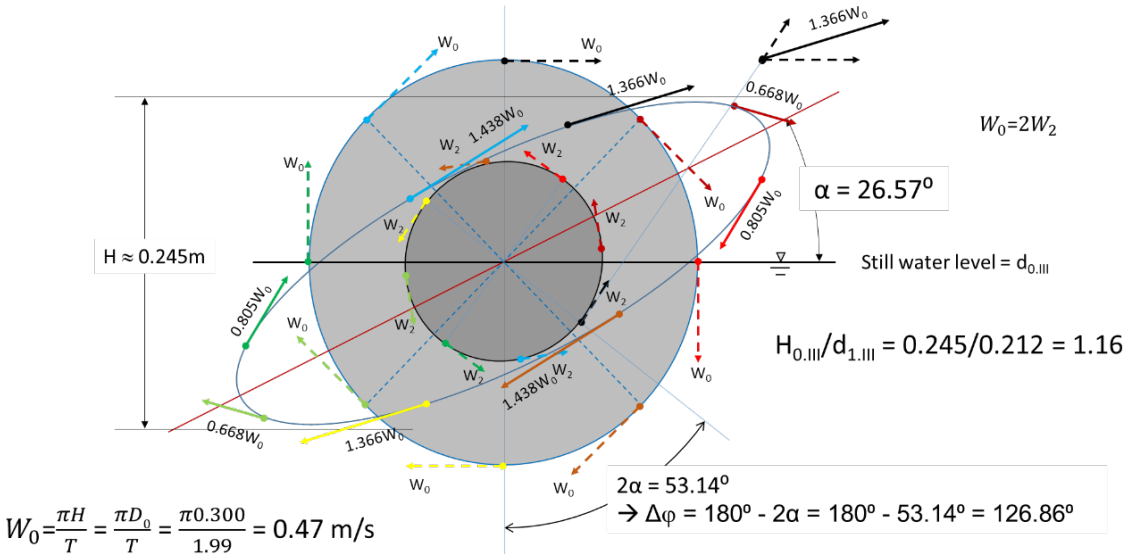

Fig. 15: Graphical determination of the elliptical orbital paths above an inclination 1: n = 1:2 corresponding to $\alpha = 26.57^0$. Mirror axis of configuration III. Vector addition for the ratio $D_0/D_2 = 0.300m/0.152m = 1.97$ of the water level (layer depth $d_{0.III} = 0.0m$ corresponding to the coordinates $\xi = 0.212m$ and the reflection of the orbital motion at $\xi' = -0.200$ (approximate below the inclined ground), cf. Fig.12. Thus, the relationship $W0 = 1.97W_2$ applies to the circumferential velocities.

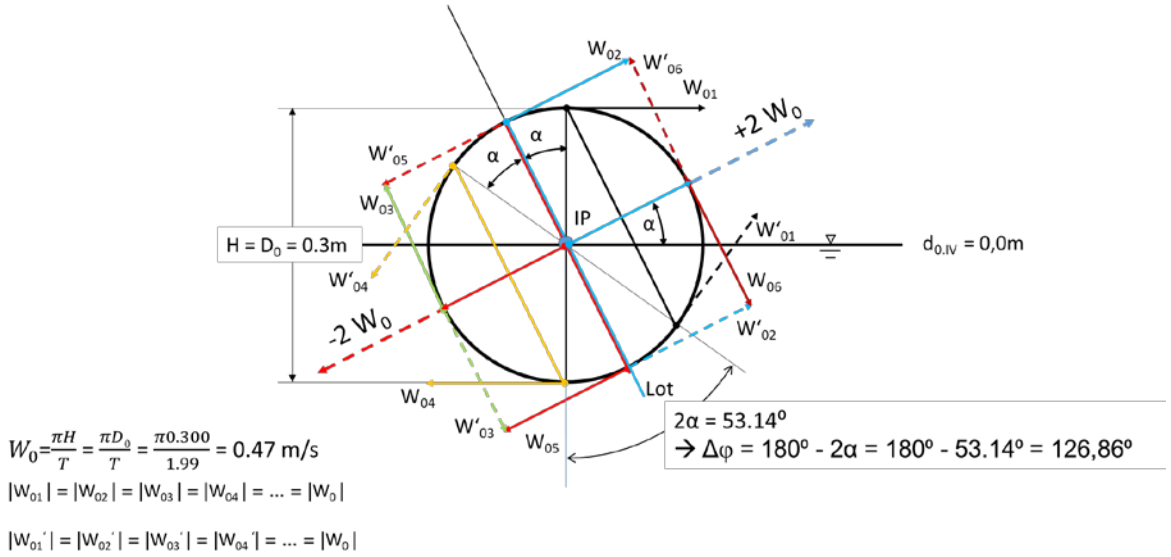

Fig. 16: Representation of the linearly polarized particle vibration at the intersection (IP) of the still water level (SWL = $d_{0.IV}$) with the slope.

When the water depth decreases inland, the reflection can be carried out at the intersection IP of the slope with the still water level (confluence of the edge streamlines of the still water level and slope) under the specification of a fictitious incident wave height, cf. Fig.16.
Referred to IP (= coordinate origin) the circular orbital velocities W_i are superimposed to the respective same-colored (dashed) opposite rotating velocities W_i', mirrored at the inclination surface. The result is a linearly polarized particle oscillation at the slope surface with maximum elongations of ± D_0 and maximum velocity magnitudes of ± $2W_0$ when swinging through point IP.

https://doi.org/10.24355/dbbs.084-202002031131-0

From the diagram it is also recognizable that in the case of an inclined mirror surface, the position vector of the mirrored point on the orbital path against the vertical starting point vector of the velocity vector W_{01} around the angle of the phase jump is: $\Delta\varphi = 180° - 2 \cdot \alpha°$ (formula 8a).
In addition, Tab. 1 shows the schema for the mathematically exact addition of the orbital velocity vectors involved in the exponentially reduced mirroring as an example for two consecutive pairs of base positions on the orbital paths of the Fig.15. The upper table concerns the base positions with the location vector angles 450° and 323.14°, and the lower table the base positions with the location vector angles 495° und 278.14°.
Thus, for the complete wave cycle in the same successive table calculations, the input angle for the bases of the incoming orbital velocities is equal to the positive amount of the selected base point angle distance (here 45°) and reduce it by the same amount for the mirrored orbital velocity. The tabular calculation is based on the decomposition of the orbital velocity vectors into their longitudinal and transversal components. The condition is that the velocity moment (made up from velocity vector and vertical distance from the coordinate origin (lever) (here: 0.743) is the same for all positions on the ellipse. The comparison of the results obtained graphically on the one hand and precisely mathematically on the other hand shows that the accuracy of the former seems quite sufficient. As an indication of this, it may also be considered that the successive, tabularly tangent inclination angles of the resulting orbital velocity vectors $\beta_1 = 17.28°$ or $\beta_2 = 32.79°$ fall below the graphically determined slope inclination $\beta \approx 26.5°$ only by -9.2° respectively exceed it by +6.29° only, cf. Fig.15.

Tab. 1: Schema for the mathematically exact addition of the orbital velocity vectors involved in the exponentially reduced mirroring (ERR).

Resulting orbital velocities on rotated elliptical orbital paths above water depth d0.III									
Vector addition for phase jump Δφ=126.86° corresponding to the slope inclination α=26.57°									
Datum = Coordinate origin (0) = Circle center. Phase point angle distances : 45°									
Phase Points	Phase point	Circumferential velocity			Phase point				
1+1' (d0.III)	angle	Magnitude πD/T	Components		coordinates				
Geschwindigkeiten	[°]	[m/s]	Xi	Yi	xi	yi	Xiyi	Yixi	Xiyi-YiXi
i=1, incident wave:	450	W0,III=1	1.000	0.000	0.000	1.000	1.000	0.000	1.000
i=2, mirrored wave:	323.14	W2,III'=W0,III/1,97	0.304	0.406	0.406	-0.304	-0.092	0.165	-0.257
Components or moment sums			1.304	0.406			0.908	0.165	0.743
Quadrates:			1.701	0.165					
Squared sums QS:			1.865						
Root QS = resulting magnitude:			1.366						
Moment M(0)= Sum (Xi*yi - Yi*xi):							0.743		
Lever=M/R:							0.544		
Equation of the resultant :		0 = M(0) +x*Ry - y*Rx y=(Ry/Rx)*x+M(0)/Rx = tanβ*x +M(0)/Rx							
		tan β = Ry/Rx:	0.31105225	arctan:	0.30157		Angle β [°]:		17.28
Tangents to the ellipse		Normal form:	y =	0.31105	x +	0.570			
		Axis segment shape:	1=	x/	-1.831	+y/	0.570		

Resulting orbital velocities on rotated elliptical orbital paths above water depth d0.III									
Vector addition for phase jump Δφ=126.86° corresponding to the slope inclination α=26.57°									
Datum = Coordinate origin (0) = Circle center. Phase point angle distances : 45°.									
Stützpunkte	Phase point	Circumferential velocity			Phase point				
2+2' (d0,III)	angle	Magnitude πD/T	Components		coordinates				
Geschwindigkeiten	[°]	[m/s]	Xi	Yi	xi	yi	Xiyi	Yixi	Xiyi-YiXi
i=1, incident wave:	495	W0,III=1	0.707	0.707	-0.707	0.707	0.500	-0.500	1.000
i=2, mirrored wave:	278.14	W2,III'=W0,III/1,97	0.502	0.072	0.072	-0.502	-0.252	0.005	-0.257
Components or moment sums			1.209	0.779	1.438		0.248	-0.495	0.743
Quadrates:			1.462	0.607					
Squared sums QS:			2.068						
Root QS = resulting magnitude:			1.438						
Moment M(0)= Sum (Xi*yi - Yi*xi):							0.743		
Lever=M/R:							0.517		
Equation of the resultant :		0 = M(0) +x*Ry - y*Rx y=(Ry/Rx)*x+M(0)/Rx = tanβ*x +M(0)/Rx							
		tan β = Ry/Rx:	0.64424723	arctan:	0.57232		Angle β [°]:		32.79
Tangents to the ellipse		Normal form:	y =	0.64425	x +	0.615			
		Axis segment shape:	1=	x/	-0.954	+y/	0.615		

https://doi.org/10.24355/dbbs.084-202002031131-0

Tab. 2: Compilation of maximum and minimum numerical orbital circle data for the mirror axes I to IV relative to the natural dimensions of the wave channel.

Compilation of numerical orbital path data										
			Mirroraxis I							
	Water-	Circle-	Orbital paths velocities					Ellipse	Wave	Comment
Indices	depth	diameter	Circle	maximum		minimum		inclined	height	
i or n	d_i[m]	D_i[m]	W_i[m/s]	Formula	Magnitude	Formula	Magnitude	β°	H|H'[m]	
					[m/s]		[m/s]			
0	0.000	0.300	0.470	±1.125W_0 horizontally	0.529	±0.875W_0 vertically	0.411	0	0.26	Fig.09
1	0.212	0.211	0.333	±1.25W_1 horizontally	0.420	±0.75W_1 vertically	0.248	0		
2	0.412	0.152	0.240	±1.5W_2 horizontally	0.372	±0.5W_2 vertically	0.120	0	0.076	Fig.08
3	0.626	0.107	0.169	±2W_3 horizontally	0.338		0.000	0		Ground
4	0.840	0.075	0.118							
5	1.040	0.054	0.085							
6	1.252	0.038	0.060							
			Mirroraxis II							
	Water-	Circle-	Orbital paths velocities					Ellipse	Wave	Comment
Indices	depth	diameter	Circle	maximum		minimum		inclined	height	
i or n	d_i[m]	D_i[m]	W_i[m/s]	Formula	Magnitude	Formula	Magnitude	β°	H|H'[m]	
					[m/s]		[m/s]			
0	0.000	0.300	0.470	±1.25W_0 slope parallel	0.588	±0,75W_0 slope vertically	0.353	26.57	0.26	Fig.13
1	0.212	0.211	0.333	±1.5W_1 slope parallel	0.500	±0.50W_1 slope vertically	0.166	26.57	0.19	Fig.14
2	0.412	0.152	0.240	±2W_2 slope parallel	0.480		0.000	26.57		Ground
3	0.626	0.107	0.169							
4	0.840	0.075	0.118							
			Mirroraxis III							
	Water-	Circle-	Orbital paths velocities					Ellipse	Wave	Comment
Indices	depth	diameter	Circle	maximum		minimum		inclined	height	
i or n	d_i[m]	D_i[m]	W_i[m/s]	Formula	Magnitude	Formula	Magnitude	β°	H[m]	
					[m/s]		[m/s]			
0	0.000	0.300	0.470	±1.5W_0 slope parallel	0.705	±0.W_0 slope vertically	0.230	26.57	0.245	Fig.15
1	0.212	0.211	0.333	±2W_1 slope parallel	0.666		0.000	26.57		Ground
2	0.412	0.152	0.240							
			Mirroraxis IV							
	Water-	Circle-	Orbital paths velocities					inclined	Wave	Comment
Indices	depth	diameter	linearly polarized vibrational movement						height	
i or n	d_i[m]	D_i[m]	W_i[m/s]	Formula	Magnitude	Formula	Magnitude	β°	H[m]	
					[m/s]		[m/s]			Fig.16
0	0.000	0.300	0.470	±2.0W_0 slope parallel	0.940			26.57	0	Ground

10. Systematic consideration of the orbital velocities and the water level deflections ζ depending on the relation of the seafloor inclination α or the phase jump Δφ in relation to the water surface.

With the intention of presenting the formalism of the "exponentially reduced mirroring" (ERR) method for the whole range of eligible seabed inclinations between 0° and 90° ($0 \le \alpha \le 90$) or distinguishing between positive or negative reflection, in the following, the subdivision of the regular wave cycle to 16 phase points with angular distances of 22.50, already used for the tabular calculations is now generally used.

https://doi.org/10.24355/dbbs.084-202002031131-0

Thus, the angle of division 22.5° differs only slightly from the actual slope angle α = 26.57° of the slope examined in the model on the one hand, and thus fits sufficiently precisely with the consideration of the subsequent intended systematic examination of slope inclinations with multiples of 22,5°.

Accordingly, in addition to the phase jump $\Delta\varphi = 135^0$ ($\alpha = 22.5^o$), which is discussed in Fig.18, the phase jumps of $\Delta\varphi = 90°$ ($\alpha = 45°$) and $\Delta\varphi = 45°$ ($\alpha = 67.5°$) are also considered in more detail, as well as their classification with regard to positive or negative Clapotis waves.

For reasons of comparability, the reference to the previously used layer depths and the associated orbital circle diameters to be superimposed is maintained.

Accordingly, the shape of the ellipses thus determined (represented by the lengths of their axes) does not change, while the long main axis takes over the slope angle of the seabed (or the (vertical) edge streamline).

The extreme values of the orbital velocities given in Table 2 are therefore also valid for the steeper slopes considered.

In addition to the elliptical orbital velocities that change with the water depth (mirror depth), the profile changes at the water surface caused by the respective phase shifts are determined below.

The calculation was (also) done here for the orbital vectors and their tangents with respect to the coordinate origin. Only the plotting of the ellipse tangents and the fitting of the ellipse is therefore subject to the low inaccuracy of the drawing.

Different from the color-coded marking of the mirrored vectors used above - due to the greater division of the wave cycle to 16 phase points - for the vector pairs with equal amounts and opposite directions the same colors are used; for example, black for the orbital vectors marked with 2 and 10, cf. Fig. 17.

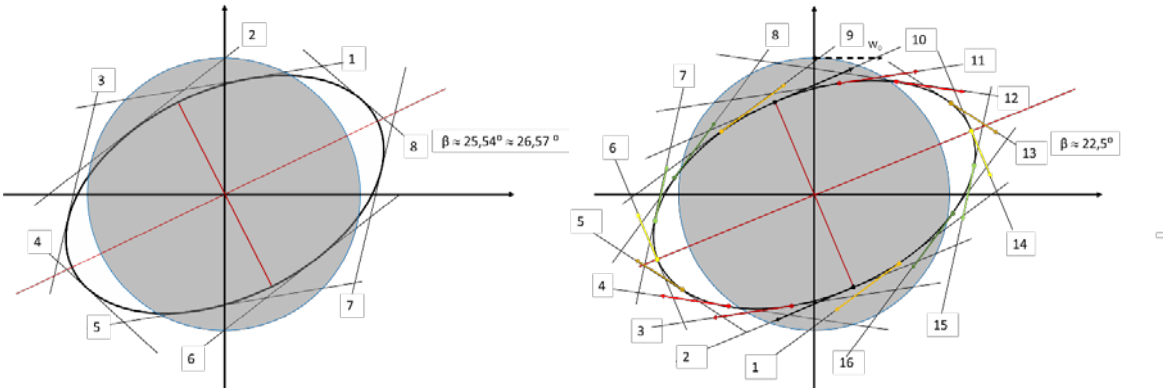

Fig.17: Comparison of only slightly different elliptical orbital paths on the surface at position $d_{0.II}$ Left: according to the ground inclination 26.57^0 with respect to the ground inclination also present in the hydraulic model, based on 8 phase points (Fig.13) and right with respect to the slightly different ground inclination 22.5^0 based on 16 phase points.

Comparable to the representations of Figures 6 and 7, the following is the consideration with respect to the continuous water depth decrease according to the seafloor inclination α = 22.5° (1:n= 1:2,414) first for the layer depths $d_{2.II}$ = 0.412m and $d_{1.III}$ = 0.212m shown in Fig.18, where

https://doi.org/10.24355/dbbs.084-202002031131-0

linearly polarized oscillation movements take place parallel to the slope as a result of the superposition of two equal opposite orbital circles.
With respect to the interference resulting from the inclination of the slope α = 22.5° (< 26.57°) the phase difference according to formula (8a) is:

$$\Delta\varphi = 180° - 2 \cdot 22.5° = 135°.$$

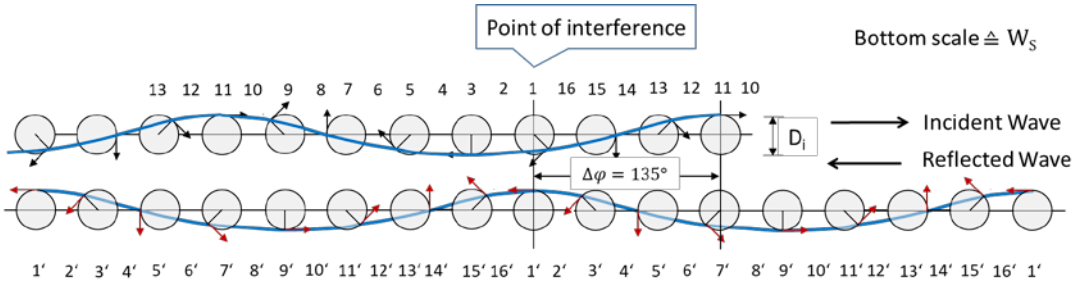

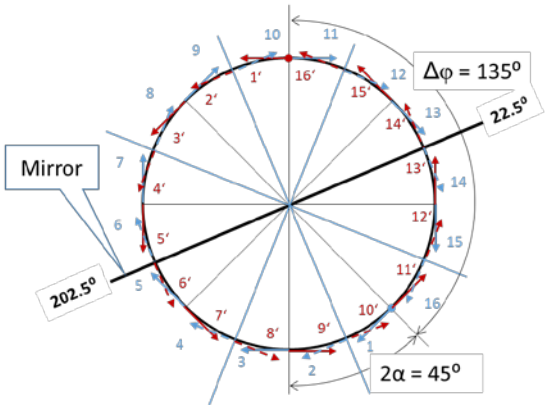

Vector	Magnitude	Direction	WLD ζ
1+1'	-1.85W_S	202.5°	0.293H/2
2+2'	-2W_S	202.5°	0
3+3'	-1.85W_S	202.5°	-0.293H/2
4+4'	-0.767W_S	202.5°	-0.541H/2
5+5'	-0-767W_S	202.5°	-√2H/4
6+6'	±0		-0.38H
7+7'	+0.767W_S	22.5°	-√2H/4
8+8'	+0.767W_S	22.5°	-0.541H/2
9+9'	+1.85W_S	22.5°	-0.293H/2
10+10'	+2W_S	22.5°	0
11+11'	+1.85W_S	22.5°	0.293H/2
12+12'	+0.767W_S	22.5°	0.324H/2
13+13'	+0.767W_S	22.5°	√2H/4
14+14'	±0		0.38H
15+15'	-0.767W_S	202.5°	√2H/4
16+16'	-0.767W_S	202.5°	0.541H/2
1+1'	-1,85W_S	202,5°	0,293H/2

Fig. 18: Due to the inclination 202.5^0 or 22.5^0 (< 26.57°) the horizontal reflection with phase jump of $\Delta\varphi = 135°$ (>126.86°) results in a linearly polarized oscillation on the ground in the layer depths $d_{2.II}$ = 0.412m and $d_{1.III}$ = 0.212m .

The computational addition of the velocity vectors on the illustrated orbital circuit is again carried out analogously to that of the already treated above phase differences (phase jumps) taking into account the relevant rotation angle of the reflected compared to the incoming orbital vectors of the wave.
Thus, for all continuous oscillation phases of a wave cycle on the ground, the expected result of a linearly polarized oscillation at the angle of the flow boundary with the angle according to formula (8b) is:

$$\alpha = 90° - 0.5\Delta\varphi = 22.5°(or\ \ 202.5°), \text{ cf. Table in Fig.18}$$

11. Analytical treatment of the phase jump depending on the variable inclination of the slope

Taking into account the phase difference Δφ on the one hand and the exponentially reduced mirrored orbital circle diameter on the other, the resulting water level deflections ζ_{res} and the magnitudes W_i which are based on the elliptical or on the linearly polarized orbital path velocities, can

https://doi.org/10.24355/dbbs.084-202002031131-0

also be determined formally by superimposition of properly phase-shifted cosine functions. This was done here by using the table calculation, cf. Figures 19 to 23.
For this purpose, the circular orbital movement of the deep sea (the incident wave) is presumed and thus used as a scale in the sense of standardization as follows:

- Magnitude of the circular orbital velocity $W_{circ} = 1$ (= const.)
- Wave height H = 1 corresponding to water level deflections $-0.5 \leq \zeta_{circ} \leq +0.5$.

Following the concept of the ERR, the water level deflections $\zeta(d_{0.i})$ (with $I \leq i \leq IV$) result from the sums of the incoming and phase-shifted exponentially reduced mirrored orbital circle diameters. And the resulting orbital velocity magnitudes $W(d_{0.i})$ are calculated from the component sums of the incoming and phase-shifted exponentially reduced mirrored velocities.
The ordinate values obtained here as dimensionless magnitudes of unit functions can be converted at the end according to the above specified information into dimension-related wave heights or orbital velocities, cf. also Tab.2.
In order to estimate the effect of the phase jump for the entire range of practically existing slope inclinations with respect to the water level deflections, to the orbital velocity magnitudes and to the orbital paths, the following 5 figures contain the results of such calculations for slopes $\alpha = 0^o$, $\alpha = 22.5^o$, $\alpha = 45^o$, $\alpha = 67.5^o$ und $\alpha = 90^o$, each in comparison to the incident wave from deep water. This contains 5 functions related to the wave cycle for the resulting water level deflections $\zeta(d_{0.i})$ and the resulting orbital velocity magnitudes $W(d_{0.i})$. In addition there are approximate examples of the elliptical orbital paths belonging to $\zeta(d0.III)$ and the linearly polarized orbital paths belonging to $\zeta(d_{0.IV})$. Both to be compared to the circular orbital path of the specified unit-deep water wave $\zeta(d_{0.IV})$. The individual functions refer in principle locally to the intersection points of the designated mirror axis with the still water level and this in such a way that they show the (relevant) changes approaching the intersection point IP.
Because of the fact that the diameters of the orbital circles involved depend on the local water depth only, in the analysis carried out here for all selected mirror depths ξ - instead of the above-mentioned intersections - the still water level points vertically above the intersection of the ground with the respective mirror axis can also be considered to be reference points.
In order to allow an undistorted insertion of the orbital paths related to the water level into the graphs of the calculated water level deflections, the vertical scale of the water level deflections also was applied (approximately) with regard to the horizontal coordinate axis.
While in the individual graphs the considered parameters W_i, ζ_i and the corresponding orbital paths are commented on only separately in relation to the total wave cycle, in the following also a relative consideration between the 5 similar parameters of the 5 inclined slopes is carried out.
It should be noted, however, that the presentation method used for the time being does not reflect a phase-compliant representation of the functions $W_i(\beta)$ und $\zeta_i(\beta)$.
In reality, the minima of the orbital velocity magnitudes occur at the same time as the extreme values of the water level deflections ζ_i and the sign change of the water level deflections is carried out in the same phase with the maxima of the Orbital velocity magnitudes. This means that, at all inclinations, the functions of the orbital velocity magnitudes $W_i(\beta)$ in the wave cycle should appear shifted by 90^o in the direction of smaller or larger values (to the left, or right), which must be taken into account.
A closed analytical formulation, which does not require this correction, should be reserved for another article if necessary.
In the comparative analysis, the theoretical limiting cases contained in Figures 19 and 23 are preceded by the positive and negative Clapotis shown.

https://doi.org/10.24355/dbbs.084-202002031131-0

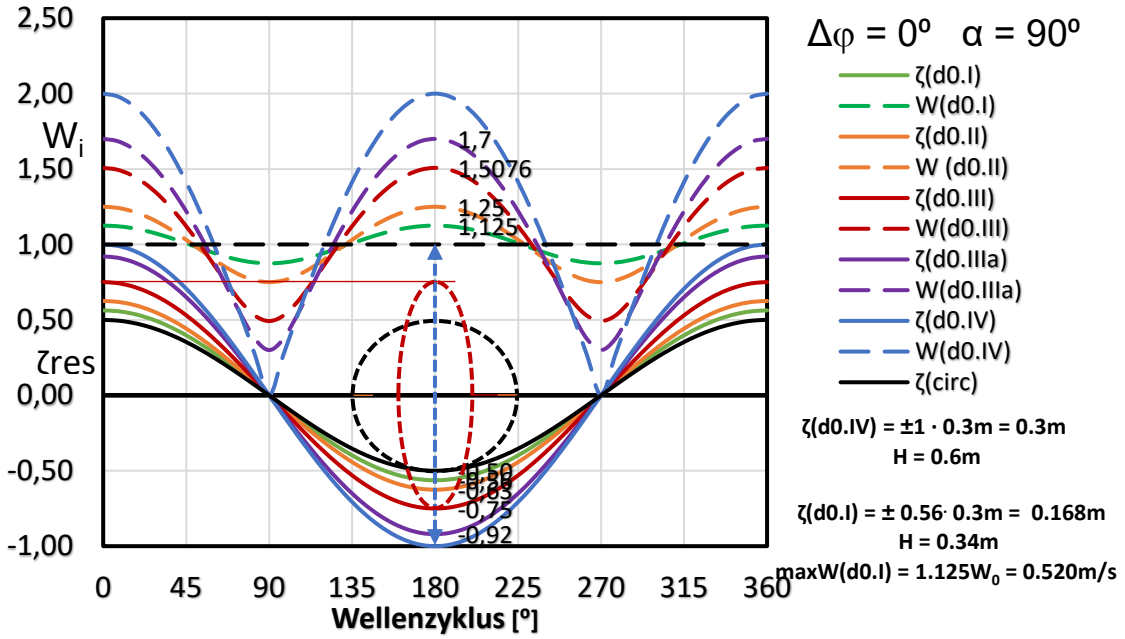

Fig. 19: Unit orbital velocity magnitudes W(d0.IV) and unit water level deflections ζ(d0.IV) for the wave cycle of a positive Clapotis over deep water ($d \geq L/2$) for the mirror depth of ξ = 0.0m (d0.IV), and 4 partially positively reflected waves ζ(d0.IIIa), ζ(d0.III), ζ(d0.II), ζ(d0.I) for the *fictional* mirror depths 0.106m, 0.212m, 0.412m and 0.626m, as well as the associated orbital paths mentioned above.
The commas in the numerical ordinate values should be read as points.

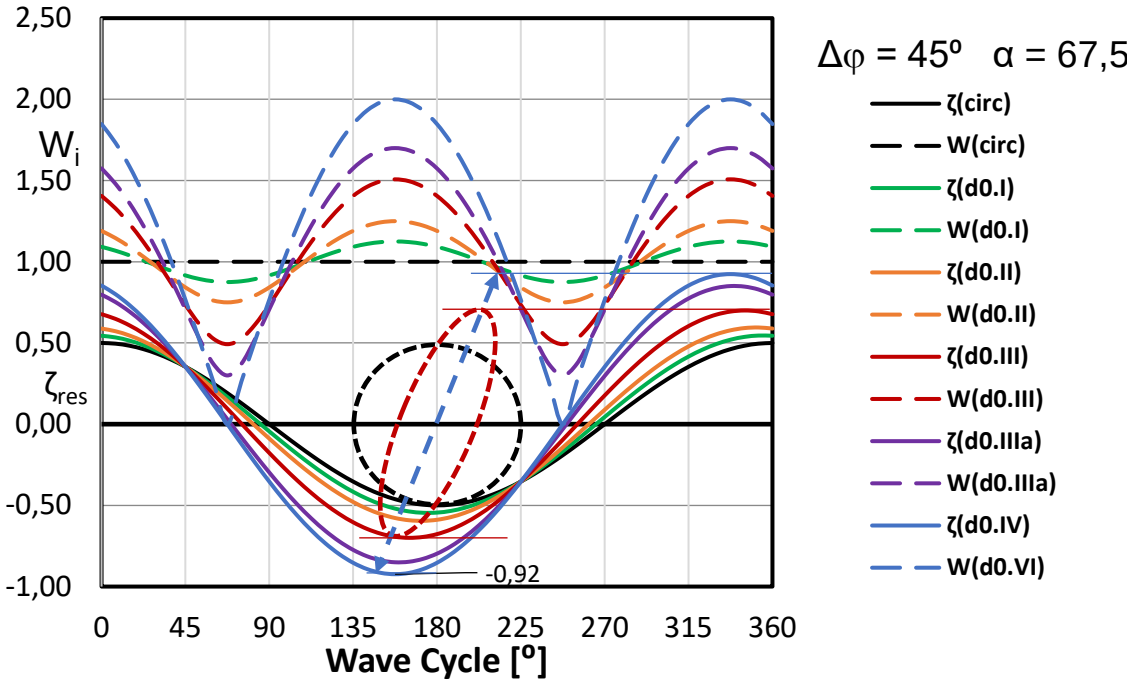

Fig.20: Unit orbital velocity magnitudes W and unit water level deflections ζ for the wave cycle of partially positively reflected waves over a flat inclination of the slope $\alpha = 67.5^0$ for decreasing mirror depths d(0.I) to d(0.IV). Orbital paths exemplify deep water (black) and mirror depths d(0.III) (red) and d(0.IV) (blue).

https://doi.org/10.24355/dbbs.084-202002031131-0

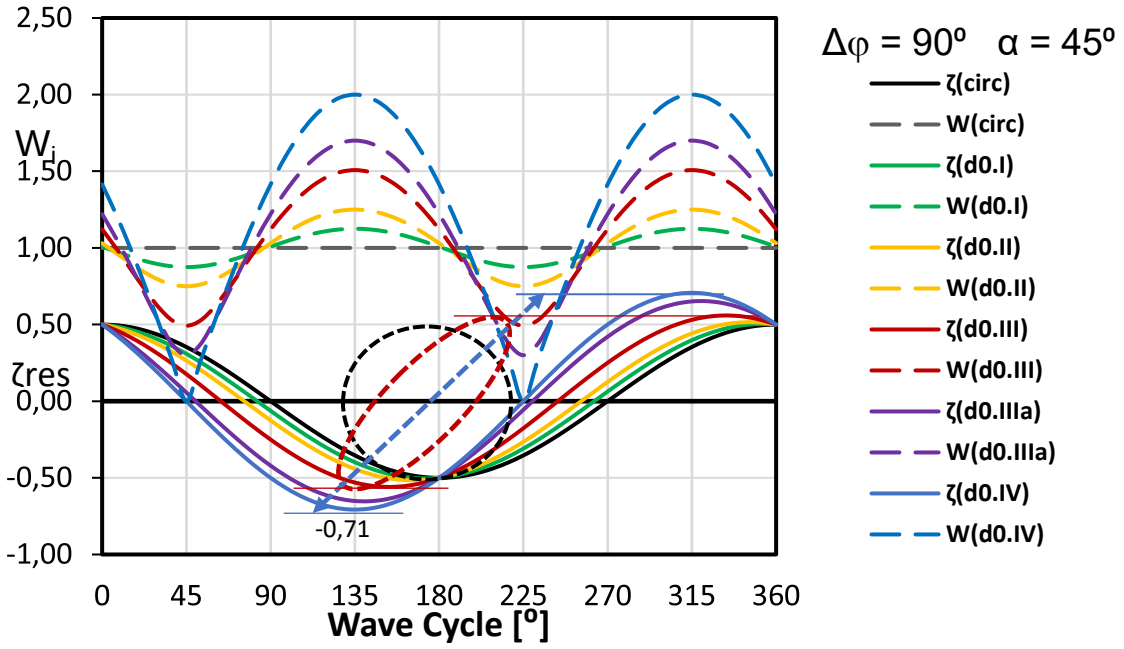

Fig. 21: Unit orbital velocity magnitudes W and unit water level deflections ζ for the wave cycle of partially positively reflected waves over a flat inclination of the slope $\alpha = 45^{o}$ for decreasing mirror depths d(0.I) to d(0.IV). Orbital paths exemplify deep water (black) and mirror depths d(0.III) (red) and d(0.IV) (blue).

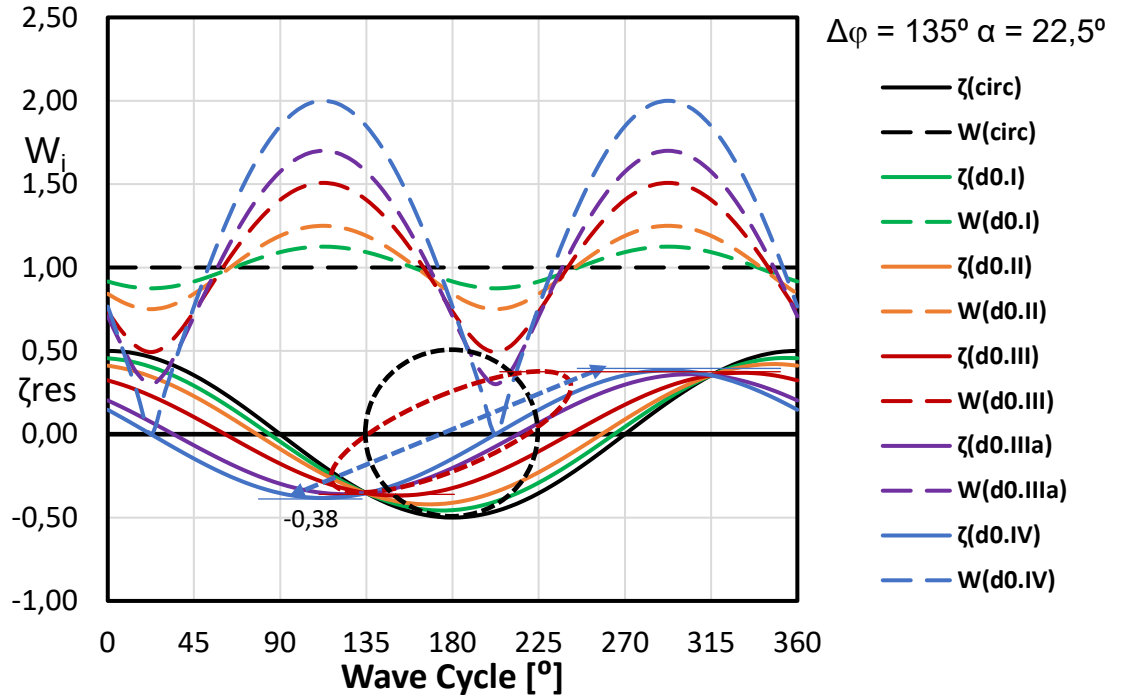

The commas in the numerical ordinate values should be read as points.

Fig. 22: Unit orbital velocity magnitudes W and unit water level deflections ζ for the wave cycle of partially *negatively* reflected waves over a flat inclination of the slope $\alpha = 22.5^{o}$ for decreasing mirror depths d(0.I) to d(0.IV). Orbital paths exemplify deep water (black) and mirror depths d(0.III) (red) and d (0.IV) (blue).

The commas in the numerical ordinate values should be read as points.

https://doi.org/10.24355/dbbs.084-202002031131-0

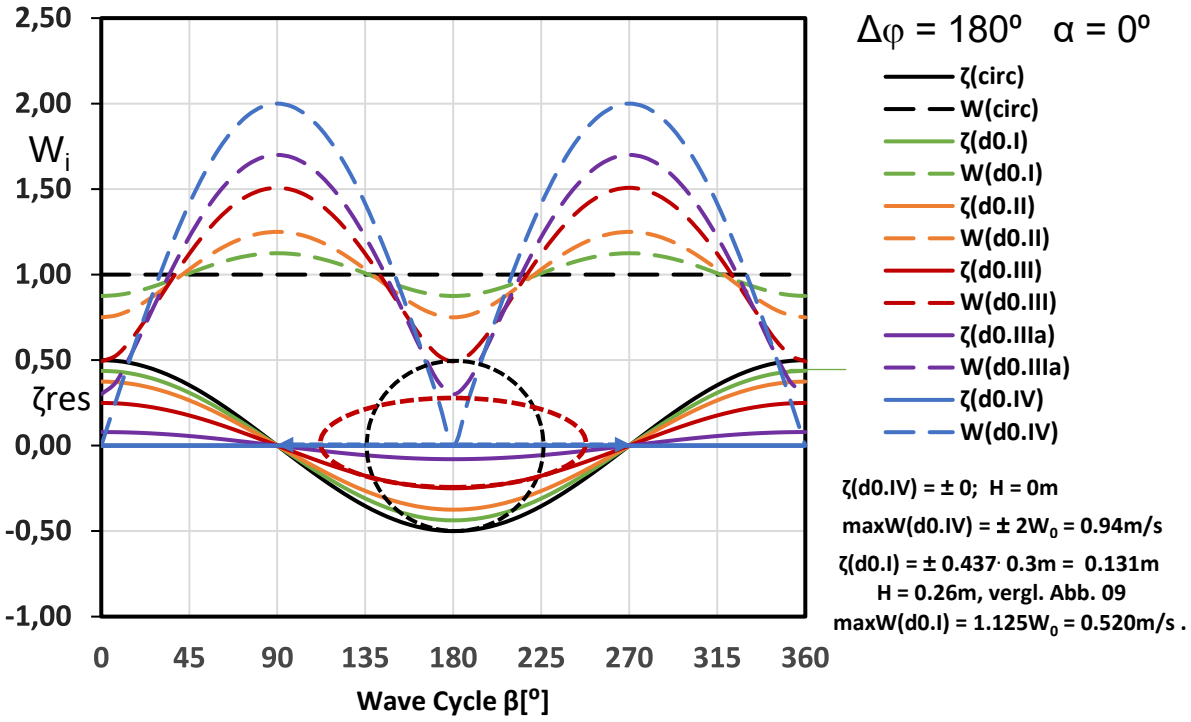

Fig. 23: Unit orbital velocity magnitudes W(d0.IV) and unit water level deflections ζ(d0.IV) = 0 for the wave cycle of the negative Clapotis ξ (d0.IV) = 0.0m for the mirror depth ξ = 0.0m (d0.IV) and of 4 partially negatively reflected waves ζ(d0.IIIa), ζ(d0.III), ζ(d0.II), ζ(d0.I), for the 4 *fictious* mirror depths 0.106m, 0.212m, 0.412m and 0.626m above flat ground, as well as the above-mentioned orbital paths, see Fig. 12
The commas in the numerical ordinate values should be read as points.

When commenting on the functions shown, it should be noted that only the orbital movements at the water surface (the layer depth d (0.i)) are shown.
The water depths d0.i used in Figures 19 to 23 are compared in the following to the mirror depths belonging to the mirror axes I to IV at the water level in the model to investigate the influence of the depth of the mirror ξ on the wave height (in particular over inclined edge streamlines).

Associated water depth	Mirror depth
of	ξ[m]
d(0.IV)	0.00
d(0.IIIa)	0.106
d(0.III)	0.212
d(0.II)	0.412
d(0.I)	0.626

In general, for all selected inclinations, the maximum oscillation amplitudes occur at the linearly polarized oscillations in the case of the mirror depth ξ = 0 parallel to the respective inclination.

https://doi.org/10.24355/dbbs.084-202002031131-0

In the case of positive Clapotis (PC), Fig. 19, this concerns the transverse particle movement on the vertical wall relative to IP. For this purpose, the respective functions are designated as d(0.IV) depending on the parameter of the layer depth.
If larger mirror depths ξ are selected, ellipses are created, whose axes grow perpendicularly to the vertical wall at the expense of the wall-parallel axes until the circular orbital movement of the incoming comparison wave is reached.
This result becomes plausible when increasing distances from the vertical wall or from the vibration antinode are considered.
The amplitudes of the water level deflections decrease from ± 1 of the pure transverse oscillation to ± 0.5 of the circular polarized oscillation and the maximum and minimum magnitudes of the orbital velocities occurring twice in the oscillation cycle change from W = 2 or W = 0 to the constant circular orbital velocity W = 1.
As an example in Fig.19, on the one hand, the elliptical orbital path belonging to ζ(d0.III) is shown- and, on the other hand the corresponding wave heights H[m] and the maximum orbital velocities W[m/s] are given for ζ(d0.IV) and for ζ(d0.I) using the above conversion data. For the functions ζ (d0. IIIa) to ζ(d0. I) it is possible to speak of partially standing positive Clapotis waves, since their two oscillation nodes with horizontal distances of $\Delta\beta = 180^{o}$ in the wave cycle are positioned also at the SWL.
On the other hand, the theoretical negative Clapotis (NC), Fig.23, is assigned a linearly polarized horizontal longitudinal oscillation with variable velocities on the ground with magnitudes varying by W = 1 between 0 and 2. Their node positions (phases of missing velocity) are not initially recognizable in the vibration cycle (as points of direction reversal), since the water level deflections (by definition) disappear over the entire oscillation cycle, ζ(d0.IV) = 0.
If larger mirror depths are selected in the same way as for the positive Clapotis, ellipses are created here, whose long axes shrink parallel to the inclination in favor of the vertically growing axes until the orbital motion of the circular polarized incoming comparison wave is reached.
This result becomes plausible if, conversely, the circular cosine wave coming in from the deep water is assumed to reach an area of decreasing water depth up to ζ (d 0.IV) = 0 at IP
Then the orbital paths first deform to the described ellipses with their axes perpendicular to the inclination decreasing and the inclination-parallel axes increasing up to IP, where there results the linear polarized oscillating movement (comparable to the washing motion present after the wave breaking).
The maximum and minimum magnitudes of the orbital velocities, occurring twice in the oscillation cycle, change from W = 2 respectively W = 0 to the constant circular orbital velocity W = 1.

As an example in Fig.23, on the one hand, the elliptical orbital path belonging to ζ(d0.III) is shown) and, on the other hand the corresponding wave heights H[m] and the maximum orbital velocities W[m/s] are given for ζ(d0.IV) and for ζ(d0.I) using the above conversion data.
For the functions ζ(d 0.IIIa) to ζ(d0.I) one can also speak about partially standing but in this case negative Clapotis waves, since also their two oscillation nodes with horizontal distances of $\Delta\beta = 180^{o}$ in the wave cycle are positioned in the SWL.

The transition from positive total reflection (Fig.19) to negative total reflection (Fig.23), due to decreasing slope inclinations, is approximated by similar calculations for the inclination angles of $\alpha = 67.5^{o}$, $\alpha = 45^{o}$ and $\alpha = 22.5^{o}$ and is documented in the Figures 20, 21 and 22.

As in the above cases, reference is made to the shift in the functions of the orbital velocity magnitudes W, the water level deflections ζ and the changes in the orbital paths.

- The functions of the orbital velocity magnitudes W(β) as well as the water level deflections ζ(β) are shifted per decrease rate of the slope of $\Delta\alpha = 22.5^{o}$ by the numerically equal phase angle in

https://doi.org/10.24355/dbbs.084-202002031131-0

the wave cycle $\Delta\beta = 22.5^{o}$, so that the total number between positive and negative Clapotis results in the phase difference of 90^{o}.

- The oscillation nodes are defined (here) as points of ζK in the vibration cycle, the coordinates of which are contained in all functions ζ(d0.i) calculated for a particular slope. Remarkably, their positions are in pairs both horizontally and vertically dependent on the predetermined inclined edge streamline, cf. Table 3 and Fig. 24.

Table 3: Vibration nodes 1 and 2 with horizontal phase angle distance of $\Delta\beta = 180^{0}$ and reciprocal positive or negative deviations from the still water level for slope inclinations $0 \leq \alpha \leq 90^{0}$ depending on the slope inclination angle.

Slope	Phase jump	Node 1		Node 2	
α[°]	Δφ[°]	β[°]	$\zeta_{K1}(\beta)$	β[°]	$\zeta_{K2}(\beta)$
90	0	90	0	270	0
78.75	22.5	67.5	0.19	247.5	-0.19
67.5	45	45	0.354	225	-0.354
56.25	67.5	22.5	0.46	202.5	-0.46
45	90	0	0.5	180	-0.5
45	90	360	0.5	180	-0.5
33.75	112.5	337.5	0.46	157.5	-0.46
22.5	135	315	0.354	135	-0.354
11.25	157.5	292.5	0.19	112.5	-0.19
0	180	270	0	90	0

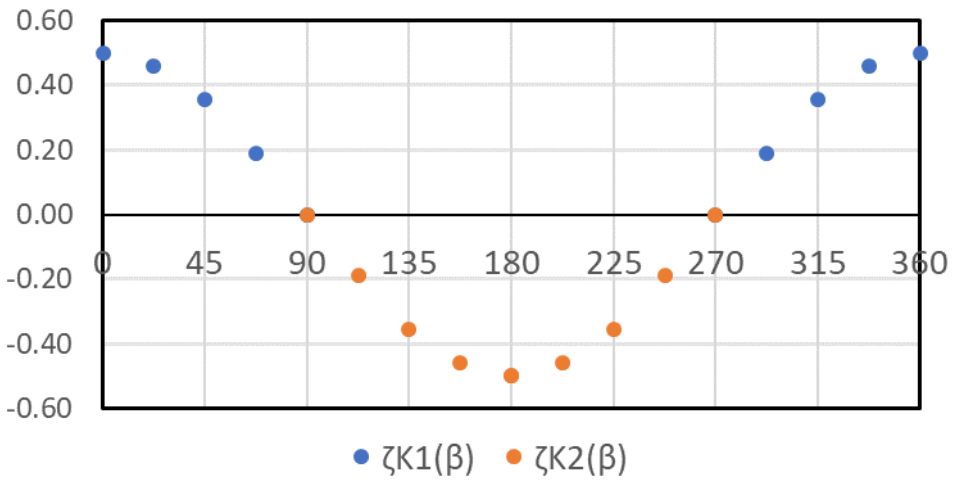

Fig. 24: Node positions relative to the still water level at slope inclinations $0 \leq \alpha \leq 90^{0}$.

- In contrast to the vibration nodes of positive and negative Clapotis waves in the still water level in Fig. 19 and 23, at the partial standing waves shown in Fig. 20 to 22, the 2 adjacent nodes with distance of $\Delta\beta = 180^{o}$ differ from the SWL by alternating negative and positive but equal

https://doi.org/10.24355/dbbs.084-202002031131-0

amounts from the still water level. This is the more the closer the inclination in question approaches the embankment angle $\alpha = 45^o$. In the latter case, the maximum node deviations are reached at the maximum node deviations of $\zeta_K = \pm 0.5$, which corresponds to the radius of the incoming circular wave.

- In the case of the positive Clapotis, the node coordinates concern non-existent (vertical) water level deflections and, in the case of the negative Clapotis, node coordinates concern non-existent (horizontal) orbital velocities in the edge streamline.
- The nodes of partially negative standing waves are exposed to magnitudes of orbital velocities with $W \geq 1$ and those of partially positive waves have orbital velocity amounts $W < 1$.

12. Wave heights H of the functions ζ(d0.I) to ζ(d0.IV) for the angles of inclination $\alpha = 67.5^o$, $\alpha = 45^o$ and $\alpha = 22.5^o$

The following tables contain the numerical parameters required for the graphical representations.

Tab. 4: Maximum amplitudes of the resulting unit water level deflections ζ (d0.i) with respect to all 5 investigated inclination angles α.

ζ(d0.i)	0°	22.5°	45°	67.5°	90°
ζ(d0.IV)	0	0.38	0.71	0.92	1.00
ζ(d0.IIIa)	0.08	0.36	0.65	0.85	0.92
ζ(d0.III)	0.25	0.37	0.56	0.7	0.75
ζ(d0.II)	0.37	0.42	0.52	0.6	0.63
ζ(d0.I)	0.44	0.46	0.5	0.55	0.56
ζ(circ)	0.5	0.5	0.5	0.5	0.50

Tab. 5: Natural-sized wave heights H[m] as a function of the mirror depth H = f(ξ) for the inclination of the $\alpha = 67.5^0$

ζ(d0.i)	ξ[m] = d	Abst. x[m] von IP	ζ_{max}	H[m]	H/d	d/L
ζ(d0.IV)	0	0.00	0.92	0.55		
ζ(d0.IIIa)	0.1045	0.04	0.85	0.51	4.88	0.03
ζ(d0.III)	0.209	0.09	0.70	0.42	2.01	0.06
ζ(d0.II)	0.418	0.17	0.60	0.36	0.86	0.11
ζ(d0.I)	0.627	0.26	0.55	0.33	0.53	0.17
ζ(circ)			0.50	0.30		

https://doi.org/10.24355/dbbs.084-202002031131-0

Tab. 6: Natural-sized wave heights H as a function of the mirror depth H = f(ξ) for the inclination of α = 45^0

ζ(d0.i)	ξ[m] = d	Abst. x[m] von IP	ζ_{max}	H[m]	H/d	d/L
ζ(d0.IV)	0	0.00	0.71	0.43		
ζ(d0.IIIa)	0.1045	0.10	0.65	0.39	3.73	0.03
ζ(d0.III)	0.209	0.21	0.56	0.34	1.61	0.06
ζ(d0.II)	0.418	0.42	0.52	0.31	0.75	0.11
ζ(d0.I)	0.627	0.63	0.50	0.30	0.48	0.17
ζ(circ)			0.50	0.30		

Tab. 7: Natural-sized wave heights H as a function of the mirror depth H = f(ξ) for the inclination of α = 22.5^0

ζ(d0.i)	ξ[m] = d	Abst. x[m] von IP	ζ_{max}	H[m]	H/d	d/L
ζ(d0.IV)	0	0.00	0.38	0.23		
ζ(d0.IIIa)	0.1045	0.25	0.36	0.22	2.07	0.03
ζ(d0.III)	0.209	0.50	0.37	0.22	1.06	0.06
ζ(d0.II)	0.418	1.01	0.42	0.25	0.60	0.11
ζ(d0.I)	0.627	1.51	0.46	0.28	0.44	0.17
ζ(circ)			0.50	0.30		

Figures 25 and Fig.26 show the resulting wave heights in question depending on the horizontal distance of IP above the respective slope.

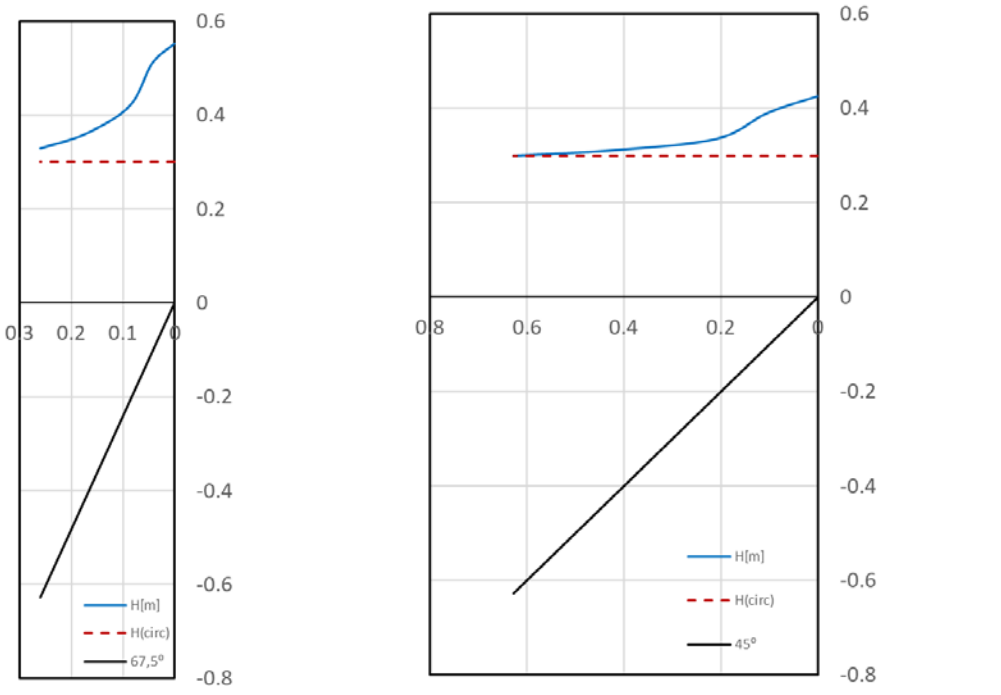

Fig.25: Wave heights H[m] above the distance of IP [m] with respect to the inclinations α = 67.5^0 and α = 45^0 (positive reflections).

https://doi.org/10.24355/dbbs.084-202002031131-0

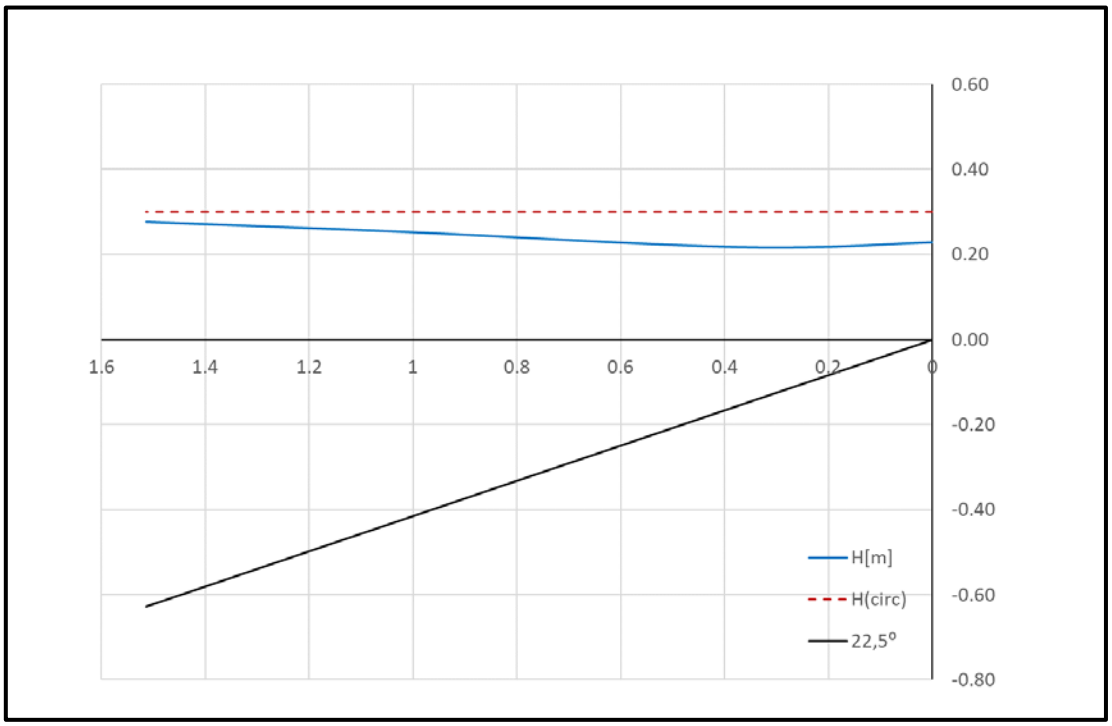

Fig.26: Wave height H [m] above the distance of IP [m] with respect to $\alpha = 22.5^{o}$ (negative reflection).

Since, on the one hand, the water level deflections (WLD) are known for the positive Clapotis assigned by $\alpha = 90^{o}$, and on the other hand, the result for the negative Clapotis (NC) does not provide water level deflections for $\alpha = 0^{o}$, the representation here is limited to the inclination angle range in between ($0^{o} < \alpha < 90^{o}$).
From the representations of the wave heights and tables 5 to 7 it can be seen that the reflection effect for the inclinations $\alpha = 67.5^{o}$ and $\alpha = 45^{o}$ rapidly decreases with the distance from IP increasing, whereas, on the other hand, it essentially increases at the inclination of $\alpha = 22.5^{o}$.
However, the wave height of the comparison wave H = 1 ($\zeta = \pm 0.5$) for deep water is approximately reached in the distance range studied only for the slope inclination of $\alpha = 45^{o}$. On the other hand, a much greater distance from the structure is required at the inclination of $\alpha = 22.5^{o}$, to which the height H(circ) of the incoming deep-water-wave is reached
According to this, it can be assumed that the maximum WLD ζres or wave heights $H \geq H_{(circ)}$ at inclinations $\alpha \geq 45^{o}$ are to be assigned to the positive reflection, cf. Fig.25. At the inclination $\alpha = 22.5^{o}$ ($\Delta\varphi = 135\ ^{o}$), however, the reflection is negative with the wave height $H < H_{(circ)}$, ,cf. Fig.26.

A more in-depth discussion, including the changed node positions (see Table 3) is not carried out here for the time being.

13. Magnitude and phase of complex reflection coefficients

In summary, the meaning of the phase jump at differently inclined edge-streamlines can be recognized also from pointer diagrams (in gaussian number plane) for the complex reflection coefficient, $\Gamma = C_r e^{i\Delta\varphi}$.

https://doi.org/10.24355/dbbs.084-202002031131-0

These were determined on the basis of the resulting functions $\zeta_{res}(d0.i, \beta)$ calculated above, as a functions of the phase shift $\Delta\varphi = 180^o - 2\alpha$, cf. formula (6a).
Such diagrams are shown on the one hand with regard to the limiting case of the linearly polarized oscillating movements in the differently inclined boundary streamlines, whereby - with regard to the ERR - reference is made to the respective point of intersection IP of the inclined boundary of the flow field with the still water level (d0.IV = level depth $\xi = 0$).
For the inclinations $0^o \le \alpha \le 90^o$ the magnitudes are obtained from $C_r = 1 \cdot \cos\Delta\varphi$ negative for slope angles $0^o \le \alpha < 45^o$ and positive for $45^o \le \alpha \le 90^o$.
So, the striking result is:
For ideally smooth slopes, theoretical complex reflection coefficients are obtained, which depend only on the preselected slope.
The angle $\alpha = 26.57°$of the slope studied in the model, corresponding to the phase shift $\Delta\varphi = 126.87°$occurs together with the magnitude $C_r = 1 \cdot \cos\Delta\varphi = 1 \cos 126.87° = -0.60$, cf. Fig 27.
For more distant positions of IP (with elliptical orbital paths) the functions ζ(d0.III) where the ratio of the orbital circle diameter $D_2/D_0 = 0.152/0.3 \approx 0.5$ is selected with respect to the surface.

Thus, the magnitudes C_r of the CRC are only about half as large, i.e. $C_r = 0.5 \cdot \cos\Delta\varphi$. For both cases, the prominent real parts of the CRC for the phase differences $\Delta\varphi = 0^o$, $\Delta\varphi = 45^o$, $\Delta\varphi = 90^o$ ($\alpha = 45^o$), $\Delta\varphi = 135^o$ and $\Delta\varphi = 180^o$ are to be seen in the respective Figures 27 or 28.

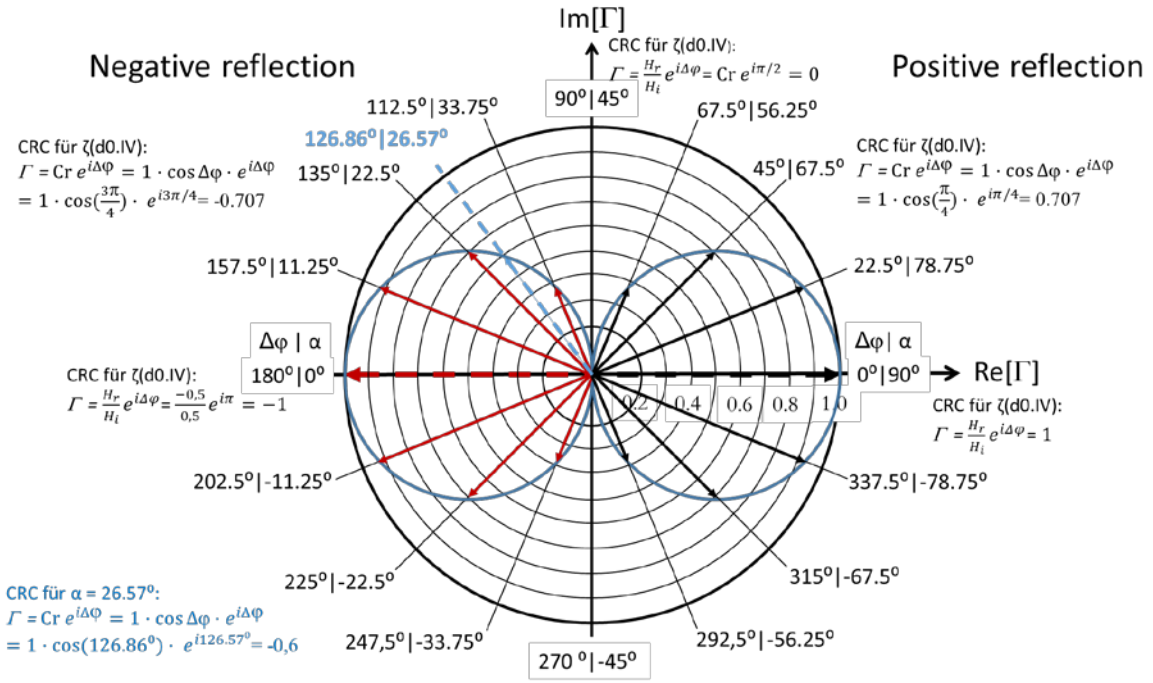

Fig. 27: Pointer diagram for the representation of complex reflection coefficients CRC $\Gamma = C_r e^{i\Delta\varphi}$ for phase jumps $0^o \le \Delta\varphi \le 180^o$ (left value) corresponding to slope angles $90^o \ge \alpha \ge 0^o$ (right value) with respect to the exponentially reduced mirroring at the intersection IP of the still water level (d0.IV) with the slope in question.

https://doi.org/10.24355/dbbs.084-202002031131-0

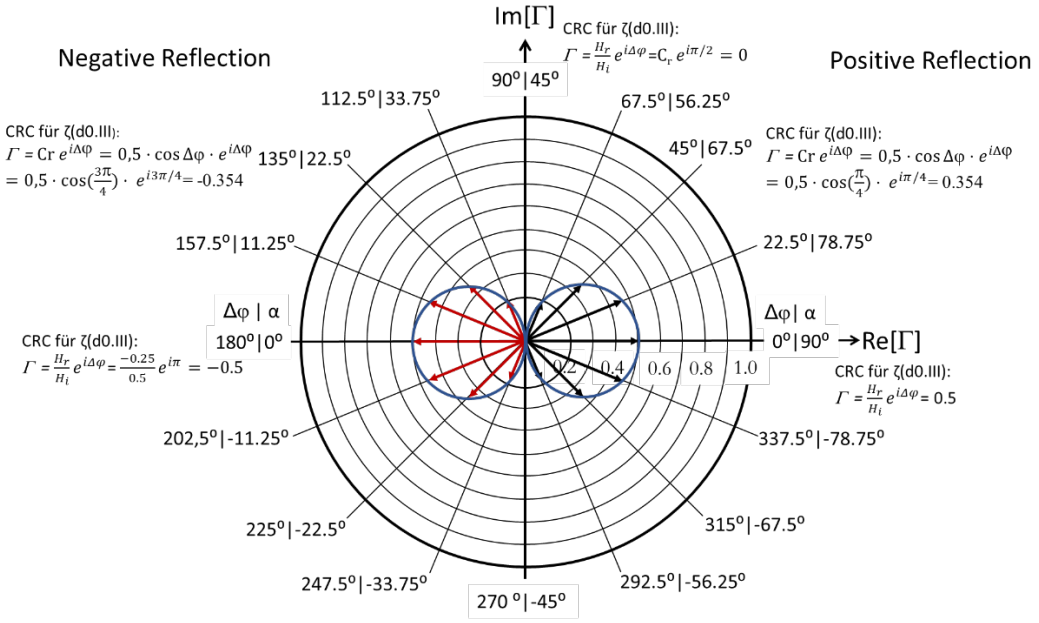

Fig.28: Pointer diagram for the representation of complex reflection coefficients CRC $\Gamma = C_r e^{i\Delta\varphi}$ for phase jumps $0^o \leq \Delta\varphi \leq 180^o$ (left value) corresponding to slope angles $90^o \geq \alpha \geq 0^o$ (right value) with respect to the exponentially reduced mirroring at the Intersection of the still water level (d0.III) with the mirror axis III.

14. Discussion and outlook

In the past, the topic of phase shift between incident and reflected waves has been dealt with empirically, mostly in connection with coastal protection structures in shallow water. The investigations of Sutherland and O'Donogue [9] can be taken as a representative example. With reference to 20 sources they come to the conclusion that the phase shift is determined by a dimensionless number χ3. The latter comprises the parameters slope inclination α, the wave period T, the water depth dt at the foot of the slope and the wave direction.

In contrast to this, in the present theoretical consideration, which is oriented on the fundamentals, the phase shift Δφ, with regard to its use in the limited water depth range, is only linearly dependent on the slope inclination.

With regard to the transferability to nature, the result should have the claim of priority consideration over the other parameters mentioned above, even if only the case of retroreflection is covered here.

As is well known, the term Clapotis has so far been used for an approximately perfectly standing wave seaward of a vertical wall (in limited water depth for d/L < 0.5). Its streamline image shows on the one hand the doubling of the wave height (to 2H) at the structure compared to the incident wave height H and shows as a second feature the maximum horizontal flow velocity at the bottom below the node of oscillation.

On the other hand, the author refers the term "positive Clapotis" more precisely only to the vertical linearly polarized transverse oscillatory motion of the water particles of the perfectly standing wave at their antinodes (or at the vertical wall) and defines it as the theoretical boundary condition in deep water.

https://doi.org/10.24355/dbbs.084-202002031131-0

The theoretical limit condition in shallow water, on the other hand, is the horizontal linearly polarized longitudinal oscillatory motion of the water particles of an advancing wave at the seafloor, which is called "negative Clapotis".

When the water depth decreases at an inclined plane, such a negative Clapotis occurs at the intersection IP of the slope inclination with the still water level, where the latter theoretically coincides.

If, in this context, the 3-dimensional orbital field in the area of decreasing water depth is regarded as an oscillating continuum whose degrees of freedom are determined by the boundaries, the restriction to the vertical plane containing the direction of progress of the incident wave is sufficient for the retroreflection considered here (especially in a wave channel).

Accordingly, two degrees of freedom can be assigned to the circularly polarized waves incident from deep water (corresponding to their two oscillations linearly polarized perpendicular to each other, cf. chapter 3). These change in their orientations as soon as ground contact becomes effective. Then the inclination of the sea floor as a boundary condition is responsible both for the development of the inclination-parallel linearly polarized particle oscillation in the boundary streamline on the sea floor and for the degree of expression of the parallel or right-angled oscillations in the current field above the boundary streamline. Accordingly, with decreasing depth the slope parallel main axes of the rotated elliptical orbital movements increase at the expense of the slope perpendicular main axes.

According to vibration theory, only those parts of the two degrees of freedom that change with decreasing depth are taken into consideration, which depend on the slope inclination α and thus on the phase shift $\Delta\varphi$. Furthermore, the number of degrees of freedom is reduced from two to one at the point IP, with the consequence that the total energy now corresponds to the linearly polarized oscillation of the negative Clapotis alone.

A significant approximation to this theoretical case can therefore only be achieved in nature if the wave transformation does not occur with a striking wave breaking process. This is most likely to be the case with the surging breaker. In the latter case, the least amount of energy is converted into turbulence and heat, with the result that it also generates the largest wave run-up. Of importance in this context is the fact that there is a coupling between the two degrees of freedom of the elliptical orbital motion [10] (Büsching, 1991).

In the case that the latter is influenced by interfering bodies (bluff bodies) on the inclined revetment surface, this is due to the mechanism of the vortex-generated losses approximately parallel and perpendicular to the inclined revetment surface.

In contrast, an even more effective wave damping is not only due to the additional deflection, entry and exit losses of the flow into and out of the cavity in question in the "Hollow Cubes" developed by the author [11], but also to the inflow into the cavity which is globally oriented *perpendicular* to the "washing movement".

With regard to the wave transformation at plane inclined reflection surfaces, it is expected that targeted systematic model investigations will fundamentally confirm the significance of the phase difference $\Delta\varphi$. between incident and reflected waves as a function of the slope inclination α.

https://doi.org/10.24355/dbbs.084-202002031131-0

15. Bibliography

[1] Büsching, F., Complex Reflection Coefficients Applied to Steep Sloping Structures, http://www.digibib.tu-bs.de Hrsg., 1. Coastlab 12, Ghent, Belgium, 17-20 September, 2012. 2. PowerPoint Presentation,, 2012.

[2] W. W. Schulejkin, Theorie der Meereswellen, D. E. Bruns, Hrsg., Akademie-Verlag Berlin, 1960.

[3] F. Büsching, „Komplexe Reflexionskoeffizienten (CRC) bei irregulären Wasserwellen an steilen Uferböschungen," Digibib TUBS: , https://doi.org/10.24355/dbbs.084-201912111303-0, 2019.

[4] F. Büsching, Über Orbitalgeschwindigkeiten irregulärer Brandungswellen, http://www.digibib.tu-bs.de/?docid=00057951 Hrsg., Mitteilungen des Leichtweiß-Instituts für Wasserbau der TU Braunschweig, H. 42, pp. 0-256;, 1974, pp. 1- 256.

[5] H. Shoemaker and J.T.Thijsse, Investigation of the reflection of waves, Third Meeting, Intern. Assoc. Hyd. Structures Res., 1949.

[6] F. Büsching, Phasensprung bei der partiellen Reflexion irregulärer Wasserwellen an steilen Uferböschungen, http://www.digibib.tu-bs.de/?docid=00056885 Hrsg., HANSA, H.5 sowie Binnenschifffahrt, H. 9 & 10, pp. 87-98 bzw. 73-77; , 2010.

[7] F. Büsching, Sturmbrandungsphänomene an der Westküste der Insel Sylt, http://www.digibib.tu-bs.de/?docid=00056466 Hrsg., DIGIB Digitale Bibliothek Braunschweig, 2015.

[8] Büsching, F., Komplexe Reflexionskoeffizienten für Wasserwellen, http://www.digibib.tu-bs.de/?docid=00047022 Hrsg., Die Küste, H.78,: Bundesanstalt für Wasserbau (BAW), 2011.

[9] J. Sutherland and T. O'Donoghue, Wave Phase Shift at Coastal Structures, Journal of Waterway, Port, Coastal and Ocean Engineering, Vol. 124, No. 2, March/April 1998, pp. 90-98., 1998.

[10] F. Büsching, Durchströmbare Böschungsstrukturen, http://www.digibib.tu-bs.de/?docid=00046743 Hrsg., Bauingenieur 66 pp.11-14; : Springer-Verlag, 1991, pp. 11-14.

[11] F. Büsching, Hollow Cubes, http://www.digibib.tu-bs.de/?docid=00054244 Hrsg., Hamburg: Schiffahrts-Verlag "Hansa", 2001.

[12] F. Büsching, Phase Jump due to Partial Reflection of Irregular Water Waves at Steep Slopes, Proc. 3rd Int. Conf. on the Application of Physical Modelling to Port and Coastal Protection, COASTLAB 2010, Barcelona, Spain, pp. Paper no. 67, pp 1 - 10; : http://www.digibib.tu-bs.de/?docid=00047044, 2010.

[13] F. Büsching, Storm Surf Phenomena at the Western Coast of Sylt Island, http://www.digibib.tu-bs.de/?docid=58824 Hrsg., Digitale Bibliothek Braunschweig, Publikationsserver der TU Braunschweig, pp. 1-32; , 2015.